# A new way to confirm meteorite impact produced planar features in quartz: combining Universal Stage and Electron Backscatter Diffraction techniques

M.H. Voorn
MSc Thesis August 2010
Utrecht University - Earth Sciences department
Structural Geology and Tectonic research group

**Abstract**

As recognised from the geological record, meteorite impact events can have a severe influence on (local) geology, climate and life. Solid evidence for these events is therefore important to obtain. The most convincing evidence comes from microstructures in quartz. Upon impact, Planar Fractures (PFs) and Planar Deformation Features (PDFs) form parallel to specific crystallographic planes in quartz. Non-impact formed (tectonic) Deformation Lamellae (DL) may be hard to distinguish qualitatively from PFs or PDFs with the optical microscope, but do not form parallel to crystallographic planes. Quantitative methods using the Universal Stage (U-Stage) on the optical microscope have therefore been applied widely to (dis)confirm this parallelism. With the method, the quartz c-axis and poles to planar features are measured and plotted. An improved technique requires so-called indexing of the measured orientations using a stereographic projection template. Even when these techniques are applied, some proposed impact structures remain debated. An important reason for this is the U-stage can not provide the full crystal orientation of quartz.

The goal of this thesis was to check the classical U-stage techniques for quantitatively confirming impact planar features in quartz, and to see whether the addition of Electron Backscatter Diffraction (EBSD, on the Scanning Electron Microscope: SEM) and Cathodoluminescence (CL, on the SEM) can provide more solid evidence. Six previously confirmed impact and three non-impact samples were studied. U-stage analysis was performed like mentioned above. EBSD (providing the full crystal orientation) and CL data (providing 2D planar feature orientations) was gathered for the same grains, combined with the U-stage data, and analysed.

Unlike previous reports, the U-stage analysis (including the indexing method) proves to give equivocal results: plots for impact and non-impact samples are similar and can not be distinguished. Indexing of combined U-stage and EBSD data gives unequivocal results: PF/PDF crystallographic planes can be confirmed (>80% correspondence) for impact sample RI37, and not (<10% correspondence) for non-impact sample SAPP2. The combination of U-stage and SEM-EBSD may therefore provide an important new technique for definitively confirming shocked quartz, hence impact. Comparison of the 2D orientation of PDFs observed by CL, with PDF poles measured by U-stage, did not provide additional information.

## 1. Introduction and background

### *1.1. General introduction*

Meteorite impacts occur and have occurred on planets and planetoids throughout our entire solar system and beyond. The Earth, although protected from many impacts by its atmosphere, is no exception. Meteorite impact sites and their remains have been recognised since the early 1800's and possibly even before, but impact was generally not regarded as a major geological process until halfway through the 20$^{th}$ century. The interest in the extraterrestrial, expressed by the various space programs, was increased, and the development of (nuclear) bombs greatly augmented knowledge on shock physics. Within only three years, between 1959 and 1962, amorphous quartz and the high pressure quartz polymorphs coesite and stishovite were discovered in both shock experiments and nature; still the most important evidence for a meteorite impact site (summarised in French, 1998; Stöffler and Langenhorst, 1994, and references therein). Ever increasing knowledge on how to correctly identify an impact site, and the development and use of new techniques (such as electron microscopy), led to a current database of 176 confirmed impact sites on the Earth (Earth Impact Database, July 2010).

With the discovery of impact sites in the last half century, the scale and significance of meteorite impact became clear. The immense speeds (20-40 km s$^{-1}$) combined with the size (up to at least 10 km in diameter) and mass (up to $10^{16}$ kg) of an impactor imply typical kinetic energies of $10^{15}$ up to $10^{23}$ J. For comparison, the total annual heat flow of the Earth is in the order of $10^{21}$ J, the largest recorded earthquake released about $1.5 \cdot 10^{19}$ J, and the largest hydrogen bomb detonation released an energy of about $2.8 \cdot 10^{17}$ J. Upon impact, the energy release is virtually instantaneous, at a concentrated location, leading to local shock pressures up to 500 GPa, shock pressures of typically 10-50 GPa in a larger volume of rock, and shock-produced temperatures over 2000 °C. With crater sizes of 10s to 100s of kilometres in diameter (200-300 km estimated for a 10 km diameter impactor), it is not difficult to imagine a meteorite impact can have drastic effects on local geology, and possible effects on a larger scale (presented numbers from French, 1998; French and Koeberl, 2010). The ejected material from an impact event may also spread around the entire globe, and the possible climate effects are even more severe. The most famous example is of course the impact-hypothesis for the Cretaceous-Tertiary (K/T) boundary mass extinction, currently accepted by most of the scientific community, and well-known to the public (Alvarez et al., 1980; Bohor et al., 1984; Bohor et al., 1987; Bohor, 1990; and later discussions).

It should be clear from the above meteorite impact should not be ignored as a geological event, thus good recognition and confirmation of impact sites and impact rocks is crucial. This thesis focuses on quantitatively comparing measurements on quartz microstructures in rock samples from various (previously confirmed) impact and non-impact sites, using and combining previously applied techniques: Universal stage (U-stage) measurements on the optical microscope and Electron Backscatter Diffraction (EBSD) and Cathodoluminescence (CL) in the Scanning Electron Microscope (SEM). The following sections first cover several distinct impact and non-impact features found in nature, comparisons, and some previous and current ways of studying suspected impact rocks. By these means, the goal of this thesis and the reasons behind it can be explained better. It is impossible and unnecessary in the light of this study to cover all aspects of meteorite impact here, and for more extensive and detailed descriptions the reader is referred to several recent overview books and papers (French, 1998; Koeberl, 2002; Gucsik, 2009; McCall, 2010; French and Koeberl, 2010).

### *1.2. Expression of impact in rocks*

After half a century of research, most authors agree on several diagnostic and non-diagnostic features (from micro- to mega-scale) for meteorite impact. The most important are summarized in table 1. Parts of this table will be discussed in more detail below. For full descriptions, the reader is referred to the more extensive literature indicated in section 1.1.

#### *1.2.1. Large structures, chemical aspects, and rocks*

A prominent effect of meteorite impact is of course impact cratering. These craters and the surrounding rocks can be indicative for impact, like on other bodies in our solar system, but the fast erosion on Earth and the action of other geological processes that form similar structures (such as volcanic craters) obscure clear craters. Therefore, these structures are unsuitable as a direct diagnostic criterion for impact, and can thus only be used as additional information next to features that are regarded diagnostic (French, 1998; French and

**Table 1** Shock-produced deformation effects: diagnostic and non-diagnostic

| A. Diagnostic indicators for shock metamorphism and meteorite impact |
|---|
| 1. Preserved meteorite fragments [1.2.1] |
| 2. Chemical and isotopic projectile signatures [1.2.1] |
| 3. Shatter cones [1.2.1] |
| 4. High-pressure (diaplectic) mineral glasses [1.2.2] |
| 5. High-pressure mineral phases [1.2.2] |
| 6. High-temperature glasses and melts [1.2.2] |
| 7. Planar fractures (PFs) in quartz [1.2.3.2] |
| 8. Planar deformation features (PDFs) in quartz [1.2.3.2 & 1.2.3.3] |
| 9. Basal Brazil twins in quartz [1.2.3.4] |

| B. Non-diagnostic features produced by meteorite impact and by other geological processes |
|---|
| 1. Circular morphology [1.2.1] |
| 2. Circular structural deformation [1.2.1] |
| 3. Circular geophysical anomalies |
| 4. Fracturing and brecciation [1.2.1] |
| 5. Kink banding in micas |
| 6. Mosaicism in crystals |
| 7. Pseudotachylite and pseudotachylitic breccias [1.2.1] |
| 8. Igneous rocks and glasses [1.2.1] |
| 9. Spherules and microspherules |
| 10. Other problematic criteria |

More detailed sections indicated in brackets. Table after French and Koeberl, 2010

Koeberl, 2010). One of those convincing lines of evidence for impact consists of fragments of the meteorite itself, spatially associated with a suspected crater. Such an association is unfortunately rarely found, and even then often debated (French and Koeberl, 2010). Less exceptional are geochemical and isotope signatures resulting from the meteorite. The most famous example is again the K/T-boundary extinction evidenced by, among others, positive anomalies in the abundance of the platinum-group element Iridium, which is rare on Earth, and is therefore thought to be of cosmic origin (Alvarez et al., 1980). However, also this presumed evidence has been debated thoroughly in the last decades.

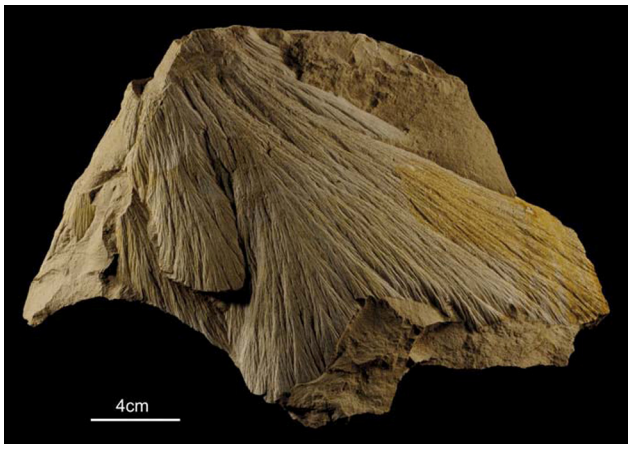


**Figure 1** Example of a group of shatter cones from the Steinheim structure, Germany. From: French and Koeberl, 2010.

On hand specimen scale, the only accepted proof of impact is given by so-called shatter cones (figure 1). These cones or partial cones are made up of curved and striated fractures, ranging from cm- up to (unusual) 10 m-scale. Although capable to form in many rock types, the best examples are found in carbonates, and they are usually formed in rocks below the crater floor, indicating no extreme pressures and temperatures (of course only relative to the entire impact event) could have acted during formation. The mechanism of their formation is however still not fully understood (French, 1998 and references therein; Dietz, 1947, and consecutive research).

From a more lithological point of view, several rock types are associated with impact cratering. These rocks are termed impactites, although this terminology is not always adapted (French, 1998). A general distinction between parautochtonous (subcrater and crater floor) and allogenic (within the crater) rocks can be made. The parautochtonous rocks consist mainly of breccias, which by themselves are not considered diagnostic for impact. The same goes for pseudotachylites and pseudotachylite breccias. The allogenic rocks are categorised mainly by the amount of melting involved. First of all, non-molten lithic breccias are widespread in craters. This is followed by melt-fragment breccias called suevites, which consist of rock and mineral fragments together with bodies of melt, in a finer-grained matrix of similar materials.

An even higher degree of melting leads to melt-matrix breccias or impact-melt breccias, where the matrix consists of melt and makes up 25-75% of the rocks. Inevitably, with ever increasing melt content, the final rock type within the allogenic group is the impact melt rock, ranging in composition between full glass and fully crystalline rock. On their own, the allogenic rocks are not considered diagnostic of impact, especially as they resemble normal igneous rocks more and more with increasing melt content. However, the more convincing evidence is usually found in the minerals and glasses within these rock types (French, 1998; Gucsik, 2009; French and Koeberl, 2010, and references therein). In section 1.2.2, some higher-pressure diagnostic features in these rocks will be covered, and in section 1.2.3, the microstructures forming at lower shock pressures (in quartz). Note there is of course a transitional region, and the pressure estimates will be regarded in further detail in section 1.2.4.

*1.2.2. Glasses, melts and phase transitions*

At pressures just above those where planar microstructures form in quartz and other minerals (sections 1.2.3 and 1.2.5), the same minerals form distinct amorphous (glassy) phases, termed diaplectic or thetomorphic glasses. No actual melting occurs during this process, and the glasses can therefore readily be distinguished from glasses resulting from melting. When melting does occur, the (geologically speaking) extremely high temperature can result in the formation of silica glass termed lechatelierite, present in molten rocks or in bands (termed schlieren) in glassy bodies. Both diaplectic glasses and lechatelierite are considered diagnostic for impact (e.g. French and Koeberl, 2010, and references therein; Gucsik, 2009).

The high shock pressures on impact may also lead to the formation of high-pressure polymorphs of minerals that normally cannot be formed at the Earth's crust. The main phases used in impact recognition are stishovite and coesite (quartz polymorphs), and diamond (graphite polymorph). Unfortunately, coesite and diamond are also found in non-impact geological settings around the world, when transported (meta-stably) to the surface from deep mantle environments. Stishovite is less abundant in other settings, as in normal equilibrium, it only forms at pressures over 10 to 15 GPa, after coesite. Upon impact, the order of polymorph formation is switched, and stishovite is thus formed at lower pressures than coesite. The occurrence of coesite, diamond and especially stishovite can thus be an important indication of impact, and is usually considered diagnostic in a supporting way (i.e. combined with other evidence) (French and Koeberl, 2010; French, 1998).

*1.2.3. Microstructures in quartz*

*1.2.3.1. Why quartz?*

By far the most convincing and accepted evidence for meteorite impact comes from shock metamorphism in quartz. As discussed previously, at high shock pressures polymorphs and distinct glasses and melts may form after this mineral, but when still in its normal crystal form, shocked quartz often displays other features as well. Although shock effects have been observed in other minerals (section 1.2.5), quartz has gained much more attention and proves to be of great use for several reasons. First, quartz is, after feldspar, most abundant in many different rock types and therefore in many target rocks. Secondly, quartz displays the greatest variety in shock effects of all minerals. Third, the shock effects are present over a wide range of pressures in a consecutive manner, making quartz suitable as a shock barometer. Fourth, quartz is quite stable and resistant to erosion, and therefore able to retain structures over time. Finally, the relatively simple hexagonal crystal structure of quartz, as shown in figure 2, simplifies measurements (Stöffler and Langenhorst, 1994; Grieve et al., 1996; French and Koeberl, 2010).

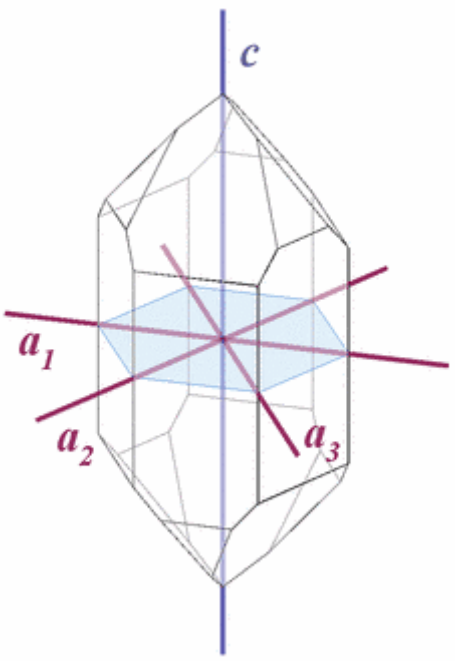


**Figure 2** Schematic representation of the crystallographic axes of the hexagonal crystal system in a quartz crystal. From: QuartzPage.de

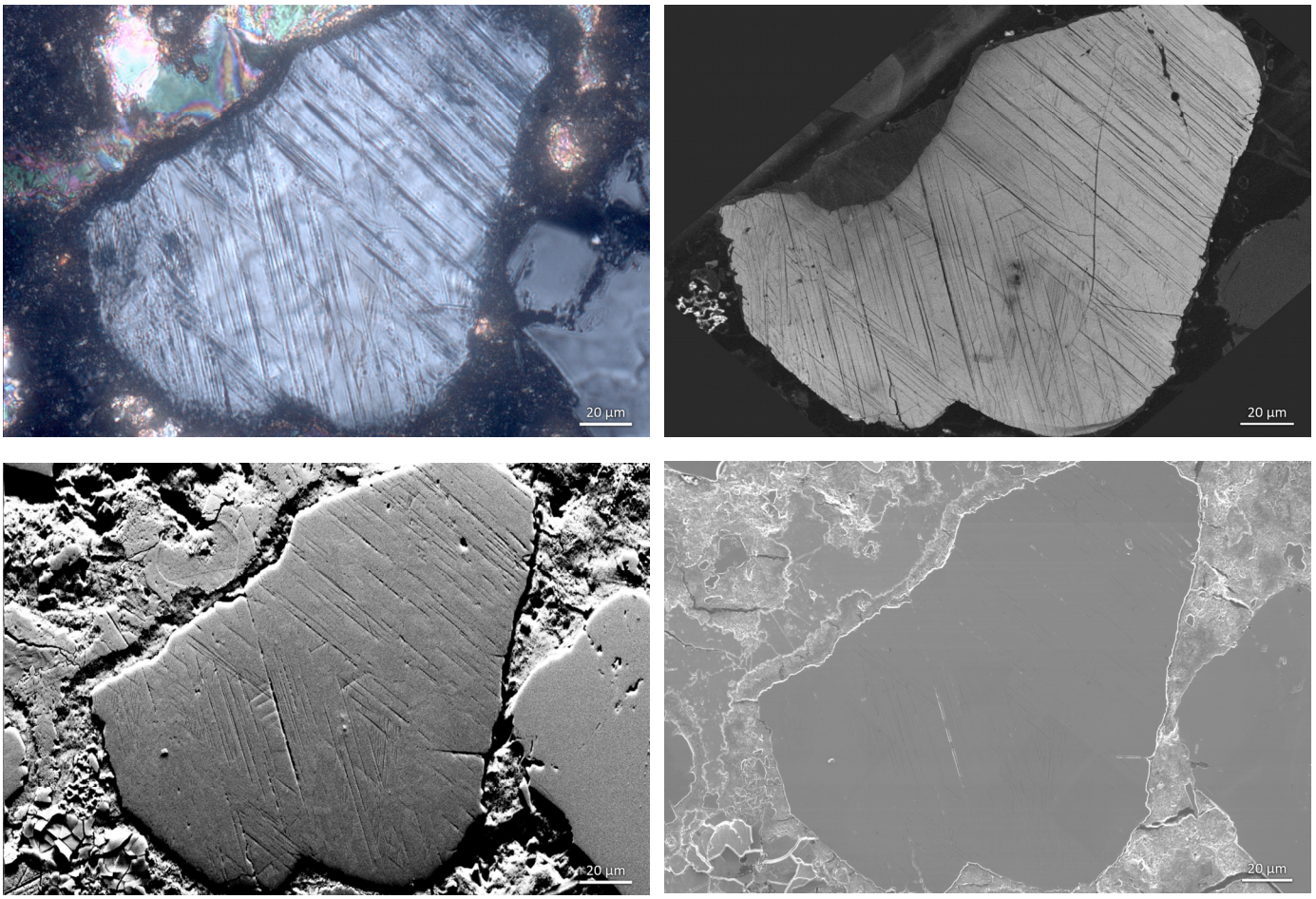


▲**Figure 3a** Different microscope images of a grain in impact sample OTT2. Clockwise, starting at top left: 1) Light microscope, cross polarised light/XPL. 2) SEM, Cathodoluminescence/CL. 3) SEM, Forescatter/FS. 4) SEM, Secondary Electrons/SE. Images courtesy of M.F. Hamers.

▼**Figure 3b** Examples of microstructures in quartz under the light microscope. Clockwise, starting at top left: 1) Multiple clear PDF sets in impact sample RI37. 2) Clear DL in non-impact sample SARB3 (similar to the investigated sample SARB2). 3) Curved (more DL-resembling) PDFs in impact sample MRO5. 4) Relatively straight, narrow (more PDF-resembling) DL in non-impact sample SARB3. The last two images illustrate the difficulty in qualitatively distinguishing DL and PDF. Images courtesy of M.F. Hamers

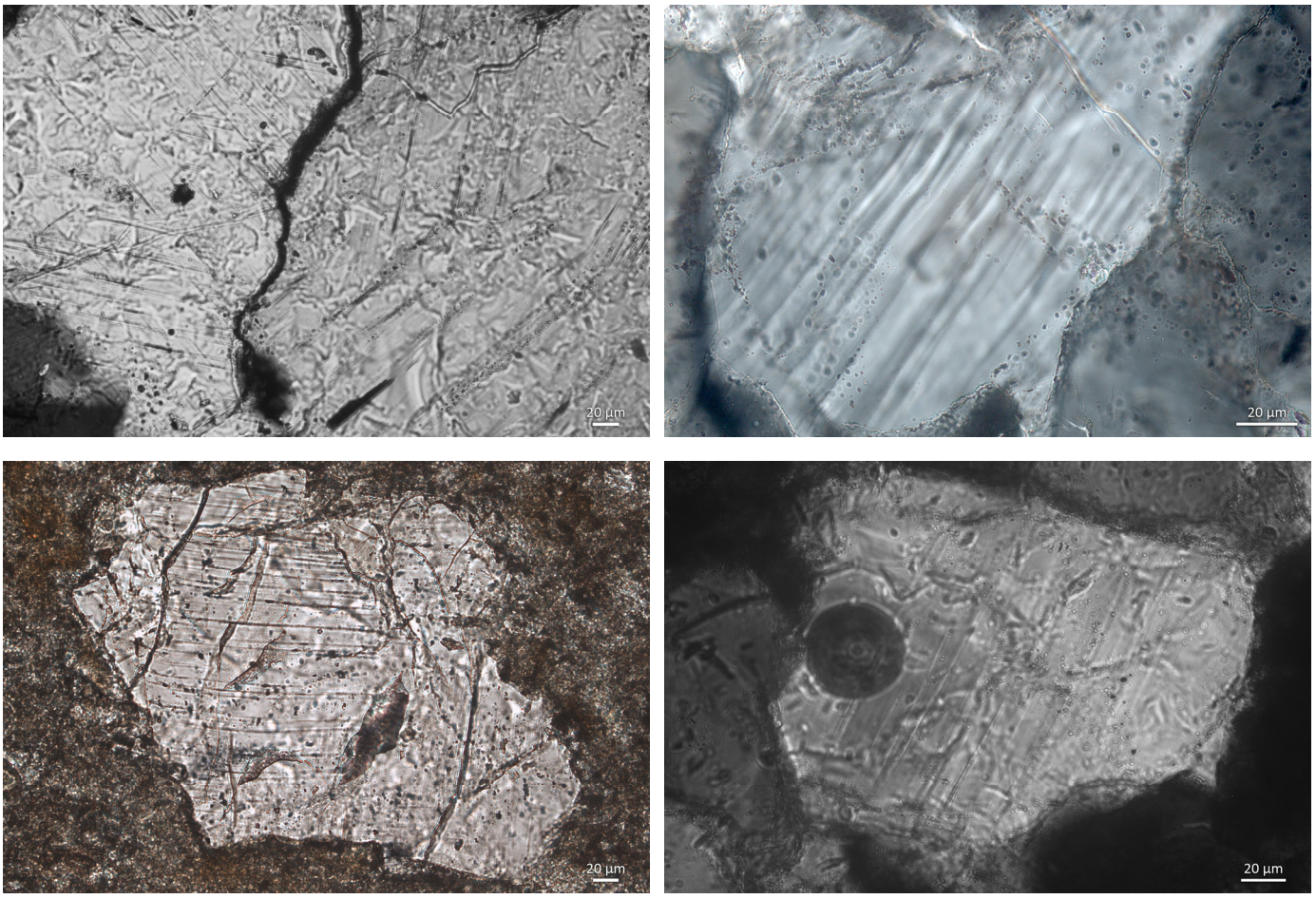

*1.2.3.2. Planar features: PFs and PDFs*

Two different types of impact planar features occur in quartz: Planar Fractures (PFs) and Planar Deformation Features (PDFs). PFs are open fractures with a width of about 5 to 10 µm, that occur in parallel sets, spaced approximately 20 µm. Generally, PFs are not curved or only slightly, and multiple sets (usually 2-3) per grain may exist. As PFs (like PDFs) occur parallel to certain rational crystallographic planes in the quartz lattice, they are "linked" to a certain grain and thus will not cross grain boundaries. The most common orientations are (0001) and {10-11}. PFs resemble cleavage in quartz, so the presence of PFs alone is not considered fully diagnostic for shock. However, when parallelism to certain planes is confirmed and/or when PFs are accompanied by PDFs (as they usually are), PFs are still considered diagnostic (French, 1998; French and Koeberl, 2010, and references therein). Finally, PFs are found to act as "grain boundaries" to PDFs (i.e. PDFs do not intersect PFs), and PFs are therefore believed to form first (Stöffler and Langenhorst, 1994).

PDFs (examples shown in figure 3), are thinner (about 1-3 µm) and much closer spaced (2-10 µm) than PFs. PDFs are not open, not curved (although sometimes they can be, probably resulting from later non-impact deformation), fully parallel to each other, and may form up to 15 (Grieve et al., 1996) or 18 (von Engelhardt and Bertsch, 1969; Stöffler and Langenhorst, 1994) different sets per grain. PDFs again do not cross grain boundaries, as they are parallel to certain rational crystallographic planes in the quartz lattice. These planes are shown in table 2. The most common planes or plane families for PDFs to form along are {10-13}, {10-12} and (0001), several others occur occasionally, and the rest is quite rare (e.g. Stöffler and Langenhorst, 1994; Grieve et al., 1996; French and Koeberl, 2010; French, 1998).

With the optical light microscope, PFs are visible as small open fractures, and PDFs as tiny filled lamellae (when abundant PDFs are present) or as traces of small (typically 1-2 µm diameter) fluid-filled inclusions: so-called decorated PDFs (e.g. Stöffler and Langenhorst, 1994; French, 1998). This has been used already quite early in the meteorite impact research (e.g. von Engelhardt and Bertsch, 1969), to identify and measure orientations of shocked quartz (using the U-stage, see section 2.1.2). Later Transmission Electron Microscope (TEM) and other electron microscopy studies have shown more PDF sets per sample are sometimes visible than with the optical microscope, and the amorphous nature of the PDFs was confirmed. Up to date, TEM studies are therefore the only definitive proof PDFs are present in quartz, although in many cases stated to be not really necessary, when enough other evidence is available (Vernooij and Langenhorst, 2005).

**Table 2** Typical crystallographic orientations of PDFs in shocked quartz

| # | Symbol | Miller-Bravais indices {*hkil*} | Polar angle (°) | Azimuthal angle (°) | Crystallographic form | No. of symmetrically equivalent planes |
|---|---|---|---|---|---|---|
| 1 | c | (0001) | 0.00 | – | Basal pinacoid | 1 |
| 2 | ω, ω' | {10-13}, {01-13} | 22.95 | 30 | Rhombohedron | 3 |
| 3 | π, π' | {10-12}, {01-12 } | 32.42 | 30 | Rhombohedron | 3 |
| 4 | r, z | {10-11}, {01-11} | 51.79 | 30 | Rhombohedron | 3 |
| 5 | m | {10-10} | 90.00 | 30 | Hexagonal prism | 3 |
| 6 | ξ | {11-22}, {2-1-12} | 47.73 | 60 | Trigonal dipyramid | 3 |
| 7 | s | {11-21}, {2-1-11} | 65.56 | 60 | Trigonal dipyramid | 3 |
| 8 | – | {21-31}, {3-2-11}, {3-1-21}, {12-31} | 73.71 | 50 | Trigonal trapezohedron | 6 |
| 9 | x | {51-61}, {6-5-11}, {6-1-51}, {15-61} | 82.07 | 40 | Trigonal trapezohedron | 6 |
| 10 | a | {11-20}, {2-1-10} | 90.00 | 60 | Trigonal prism | 3 |
| 11 | – | {22-41}, {4-2-21} | 77.20 | 60 | Trigonal dipyramid | 3 |
| 12 | – | {31-41}, {4-3-11}, {4-1-31}, {13-41} | 77.91 | 45 | Trigonal trapezohedron | 6 |
| 13 | t | {40-41}, {04-41} | 78.87 | 30 | Rhombohedron | 3 |
| 14 | k | {51-60}, {6-1-50} | 90.00 | 40 | Ditrigonal prism | 6 |
| e | – | {10-14}, {01-14} | 17.62 | 30 | Rhombohedron | 3 |

# = assigned number of PDF; Symbol = symbols assigned to common crystallographic planes in quartz; Polar angle = angle between pole to PDF and c-axis; Azimuthal angle = azimuth relative to the quartz a-axes; Multiply the number of symmetrically equivalent planes by the amount of Miller-Bravais indices to get the number of times the plane is represented in the NSPT (figure 10). Table after Ferrière et al., 2009

*1.2.3.3. Formation of PDFs and decorated PDFs*

The first models for PDF formation considered PDFs as glide planes in the crystal (von Engelhardt and Bertsch, 1969). Later TEM studies however were not in line with this interpretation. Although other models have been proposed in between, currently a model involving separation of an uncompressed region from a compressed one by the travelling shock front after impact (Goltrant et al., 1992) seems most accepted. The incompatibility or misfit (in terms of lattice parameters) of the compressed and uncompressed region is compensated by forming lamellae of amorphous material behind the shock front. With further wave propagation, the lamellae grow to finally form PDFs (all as summarized in Stöffler and Langenhorst, 1994). An adaption to this model was made later (Langenhorst, 1994), considering increasing shock pressures hence shock temperatures, to explain the formation of PDFs, PDFs with some melt, diaplectic glass around PDFs, and finally lechatelierite. These different end situations are shown in figure 4.

Decorated PDFs are thought to originate from the original amorphous material in PDFs converting back to quartz, leaving traces of fluid inclusions

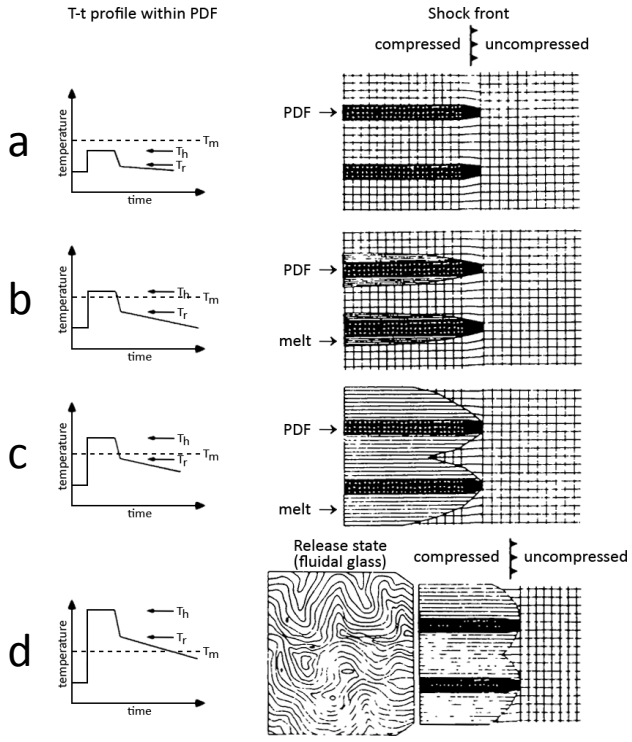


**Figure 4** Model for the formation of PDFs and consecutive stages in quartz, with increasing temperature. **a)** PDF formation only. **b)** Formation of some melt adjacent to PDFs. **c)** Formation of diaplectic glass. **d)** Formation of Lechatelierite. $T_m$ = Melting temperature of quartz; $T_h$ = Shock temperature; $T_r$ = Post-shock temperature. See text for discussion. From: Langenhorst, 1994; Stöffler and Langenhorst, 1994.

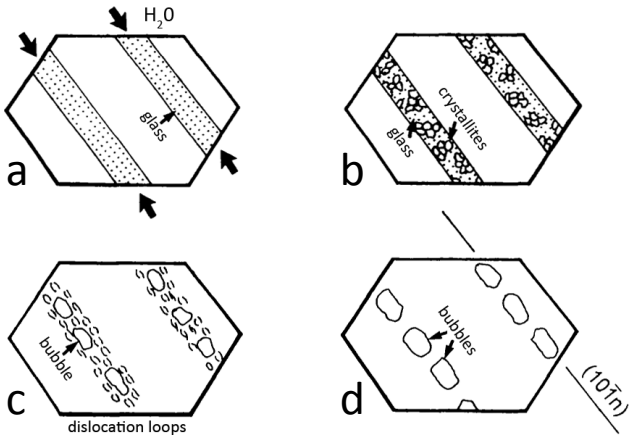


**Figure 5** Schematic representation of the development of decorated PDFs. **a)** Close to the initial state: amorphous PDFs containing $H_2O$. **b)** Recrystallisation to a mixture of glass and quartz crystallites. **c)** Exsolution of $H_2O$ from the recrystallising quartz as bubbles and adjacent dislocation loops. **d)** Final state: the original PDF is now represented by a trace of bubbles, parallel to a certain crystallographic plane. From: Grieve et al., 1996.

(summarized in French, 1998). A more detailed schematic representation of this process is shown in figure 5 (Grieve et al., 1996).

*1.2.3.4. Brazil twins*

In TEM studies, beside the nature of normal PDFs, another diagnostic planar feature in quartz was found: the basal Brazil twin. Brazil twinning is a certain type of twinning in quartz, and is usually formed by growth defects, parallel to rhombohedral planes {10-11} or {10-12} (Leroux et al., 1994; French and Koeberl, 2010). However, in shocked samples, Brazil twins were also discovered along the basal plane (0001), termed mechanical Brazil twins (Goltrant et al., 1991, 1992; Leroux et al., 1994), as they do not represent growth defects. There seems to be some uncertainty between authors whether Brazil twins should be regarded as basal PFs (e.g. Leroux et al., 1994), basal PDFs (e.g. Stöffler and Langenhorst, 1994; Grieve et al., 1996; Trepmann and Spray, 2006; Trepmann, 2008) or as a separate group (e.g. Vernooij and Langenhorst, 2005), but apart from terminology the general consensus seems to be these basal microstructures in quartz are diagnostic for shock (French and Koeberl, 2010, but already emphasised prior to TEM studies by Carter, 1965).

The formation mechanism of basal Brazil twins is most likely different from that of other PDFs, as already recognised when the model of PDF formation was created (Goltrant et al., 1992). This may also be a reason to keep Brazil twins and PDFs

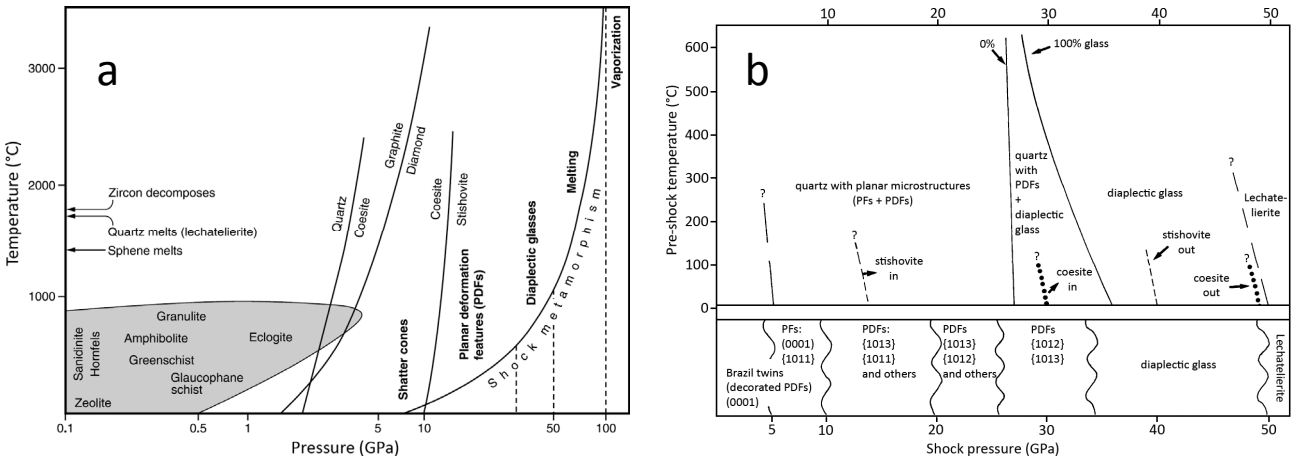


**Figure 6** Shock barometry for crystalline (non-porous) targets inferred from microstructures, phases and stages of quartz, and other lines of evidence. **a)** Full shock barometry range, showing the normal endogenic metamorphic facies for comparison. **b)** Shock barometry diagram showing the various stages of quartz in more detail, including the different types of PFs and PDFs forming at different inferred pressures. Note the difference in temperature scale between a and b. From: a) French, 1998 b) Grieve et al., 1996.

separate in terminology. The process assigned to form the basal Brazil twins is mechanical twinning, which occurs in multiple crystalline materials besides quartz. It is characterised by "very high strain rate, high deviatoric stress, and moderate temperature" (Goltrant et al., 1992). Shock experiments and comparison with nature shows these high deviatoric (or differential) stresses are only induced under relatively low shock pressures. Shock-induced differential stresses (capable of forming Brazil twins) are thus thought not to accompany shock pressures over about 20 GPa (Trepmann, 2008, 2009; Trepmann and Spray, 2006).

### *1.2.4. Shock barometry and thermometry*

One of the reasons research on quartz dominates the (microscale) research on impact metamorphism is the suitability for use as a barometer of shock pressure. In previous sections, the pressures involved and the various behaviour of quartz at different shock pressures have already been assigned briefly. Shock pressure estimates come from various sources, with an emphasis on experimental work. Note the estimates on shock pressure can be very rough! Figure 6 summarises the main evidence that can be used as a barometer for shock pressure. Table 3 shows a different representation, in terms of progressive shock stages. Here, also the decreasing refractive index with increasing shock pressure is shown. Different definitions of the shock stages exist (e.g. for quartz only or for quartzo-feldspathic rocks), but they always represent consecutive steps of increasing shock pressure (Grieve et al., 1996). Note figure 6 and table 3 might not be fully up to date with current knowledge (e.g. on additional crystallographic planes), but in the light of the goal of this thesis they represent the clearest representation.

**Table 3** Progressive stages of shock metamorphism in quartz (in non-porous rocks)

| Shock stage | | Critical sets | | Additional sets | | Optical properties of quartz (n = refractive index) |
|---|---|---|---|---|---|---|
| | | PFs | PDFs | PFs | PDFs | |
| 1 | Very weakly shocked | (0001) | (0001) | {10-11} rare | None | Normal (n ≈ 1.553) |
| 2 | Weakly shocked | | {10-13} | {10-11} , (0001) | (0001) | Normal (n ≈ 1.553) |
| 3 | Moderately shocked | | {10-13} | {10-11}, (0001) rare | {11-21}, {11-22}, (0001), {10-10}, {11-21}, {10-11}, {21-31}, {51-61} | Normal or slighly lower n |
| 4 | Strongly shocked | | {10-12}, {10-13} | Rare or absent | {11-21}, {11-22}, (0001), {10-10}, {11-21}, {10-11}, {21-31}, {51-61} | n = 1.546-1.480 |
| 5 | Very strongly shocked | | {10-12}, {10-13} | Rare | Rare | n < 1.480 |
| 6 | Extremely shocked | | | | | Diaplectic glass; n = 1.468-1.461 |
| 7 | Shock fused | | | | | Lechatelierite; n = 1.460-1.458 |

Table after Grieve et al., 1996, and references therein.

Shock thermometry involves distinct temperatures, including pre-shock, shock, and post-shock temperature. Although important for the formation of some structures or mineral phases, shock temperature estimates have received less attention than barometry. Rough estimates for shock temperature are usually derived from shock barometry results and information on melting points. For a more detailed summary, the reader is referred to Grieve et al. (1996).

Please also note the shock barometry and thermometry estimates are only valid for crystalline, non-porous targets. Porous targets are thought to behave very differently, as much more empty space is available to "withstand" impact. This of course only applies to thick sediment piles, not a relatively small top cover. Not much research has been performed on this subject (e.g. French, 1998; Grieve et al., 1996).

*1.2.5. Other minerals beside quartz*

Some other minerals beside quartz also display shock-induced features. For example, feldspar shows different shock-induced fractures, deformation bands, and PDFs. When short-spaced PDFs are combined (at an inclination) with wider-spaced features (such as albite twins), a characteristic "ladder texture" can form. Other shock-produced planar microstructures and actual PDFs have for example also been observed in pyroxene, amphibole, olivine and other minor phases (French, 1998). Minerals like olivine and graphite (mentioned before) can also develop high-pressure polymorphs upon impact (Langenhorst, 2002). Some more observed structures and pressure estimates are shown in figure 7. Due to the emphasis on quartz throughout impact metamorphism research in the last half century, and the larger abundance of clear shock effects in quartz, the rest of this thesis will only regard that mineral.

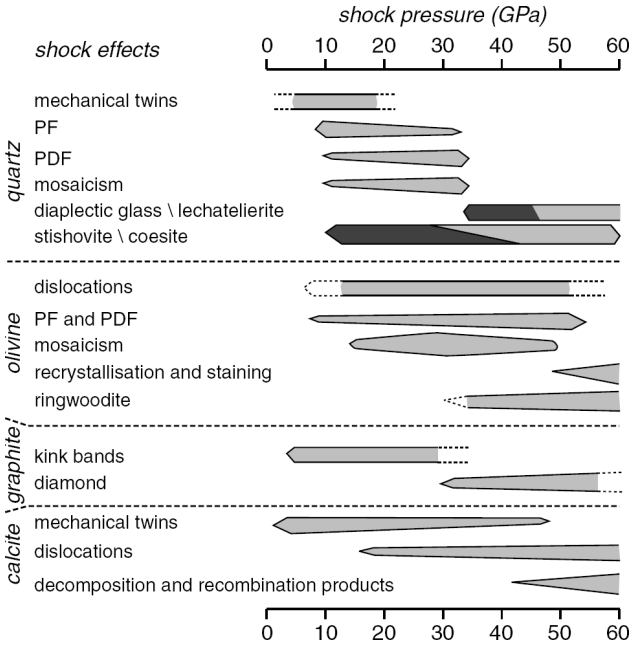


**Figure 7** Shock barometry results from shock experiments for non-porous rocks, based on certain shock effects formed in quartz, olivine, graphite and calcite. From: Langenhorst, 2002.

*1.3. Non-impact produced planar microstructures*

*1.3.1. Qualitative description and comparison to PFs/PDFs*

As mentioned in previous sections, for example large-scale craters and smaller-scale melts can not be used as diagnostic features for meteorite impact, as other geological processes (endogenic processes) are capable of forming similar structures. Unfortunately, other geological processes (mainly tectonic deformation), are also capable of forming planar microstructures in quartz, the most convincing evidence for impact metamorphism. Some linear features, such as (healed) fractures, growth lines or non-basal twinning in quartz, may sometimes be misinterpreted as impact planar features, but are generally readily distinguishable (e.g. French and Koeberl, 2010). On the other hand, tectonic (non-impact) Deformation Lamellae (DL), or Böhm lamellae (Böhm, 1883), may show similar characteristics as impact planar features. Examples of DL in samples, compared to PDFs, are shown in figure 3b. A clear description of DL and the comparison to impact-related planar features in quartz is thus important. Note the term DL is used in this thesis, as it seems to be the broadest accepted term in the scientific society (M.R. Drury, pers. comm., 2010). The term "Metamorphic Deformation Lamellae" (MDL) is also used in literature (e.g. French and Koeberl, 2010), but as this term still not stretches the endogenic nature of these lamellae, it is not used in this thesis.

DL are thought to origin from "recovery (dislocation rearrangement in low-energy configurations) after tectonic deformation" (as summarised in Goltrant et al., 1991). They are thin (usually over 2 µm) lines, spaced approximately 0.5-10 µm and higher (French and Koeberl, 2010; summary in Bruijn, 2009). DL may also be thicker (10-20 µm) and wider spaced (>20 µm) (French, 1998). Multiple bands are nearly parallel, and can be severely curved, although (near-)straight DL are not rare. The curvature is

mostly related to zones of undulatory extinction. Furthermore, DL usually have a somewhat different orientation relative to the host grain, resulting in a slightly different extinction under the optical light microscope. DL mainly occur in one set per grain, and rarely in more than two sets, and they are not related to specific crystallographic planes. In TEM studies, DL were confirmed to be internally crystalline, and usually linked to very high dislocation densities throughout the host grain (Grieve et al., 1996)

In summary, DL differ from PDFs and to some extent from PFs by:

- Thicker and more widely spaced lamellae
- Curvature and bending of lamellae instead of straight planes
- Different extinction than host grain and presence in zones of undulatory extinction
- Less parallelism of multiple planes
- Less sets per grain
- Not related to specific rational lattice planes
- Internally crystalline instead of amorphous (PDFs, not decorated), or open (PFs)
- Higher dislocation densities in the host grain

(Above after: von Engelhardt and Bertsch, 1969; Alexopoulos et al., 1988; Goltrant et al., 1991; Grieve et al., 1996; French, 1998; French and Koeberl, 2010).

*1.3.2. Quantitative comparison to PFs/PDFs*

Although the qualitative criteria in the previous section that can be addressed by optical light microscopy work can often be used to distinguish between DL and PDFs or PFs, they still might resemble each other. The main definitive proof for PDFs over the last half century has been a more quantitative analysis with the optical microscope. Using the U-stage (section 2.1.2), the relation between the quartz c-axis and (poles to) planar structures can be measured. Whereas PDFs and PFs should give angles corresponding to certain crystallographic planes, DL should display a wide range of angles, usually between ±10-30°, although larger angles are sometimes reported (von Engelhardt and Bertsch, 1969; Grieve et al., 1996). Although the most important PDF and PF orientations also fall within this range, they should display sharper and more distinct peaks at the angles corresponding to these positions, as opposed to a wider "bell-shape" for DL (summarized in e.g. French, 1998; French and Koeberl, 2010). An example is shown in figure 8. Note the bell-shape applies to a summary of data from different samples.

As it is not possible to measure the a-axes of quartz with the light microscope, inferred crystallographic planes from angular data are not necessarily correct. An improved method makes use of all the poles to planar features found in a single grain relative to the c-axis and each other. In contrast with the previous method, the azimuthal information from the U-stage measurements is also used here. By using a stereographic projection template, the poles to planar features can be "indexed" as a certain PDF-corresponding

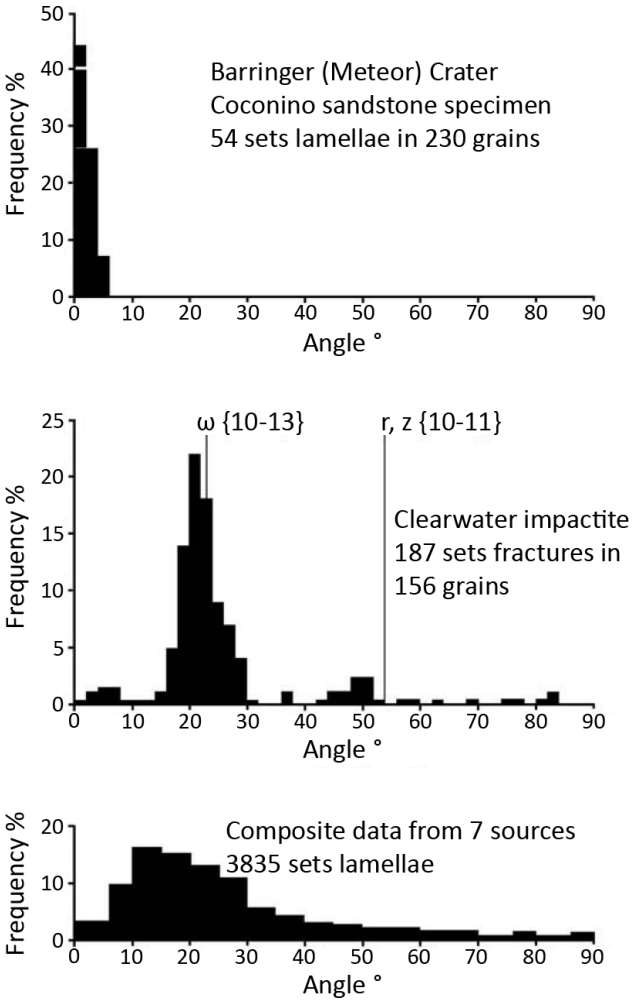


**Figure 8** Histograms of orientations of impact and non-impact planar microdeformation features in quartz grains, showing the frequency distribution of the polar angle (the angle between the quartz c-axis and the pole to the planar feature). **a, b)** The histograms for impact sites (PFs and PDFs in quartz) show clear peaks at distinct polar angles corresponding to certain crystallographic planes in the quartz crystal. 2° bins. **c)** The histogram for the non-impact samples (DL in quartz) shows a broad bell-shaped distribution without distinct spikes. Note this histogram is based on a lot more data from different sources, compared to a and b. 5° bins. From: French and Koeberl, 2010, after Carter, 1965.

crystallographic plane, or not. This method has been proposed, encouraged and improved by several authors (von Engelhardt and Bertsch, 1969; Stöffler and Langenhorst, 1994; Langenhorst, 2002; Ferrière et al., 2009; French and Koeberl., 2010), but only plotting angles directly still seems to be the most widely spread method used to date. As the method of indexing is also used in this thesis, a more detailed description follows in section 2.2.1.

*1.4. Problems in impact structure identification, and goal of this thesis*

As made clear in previous sections, the most definitive proof for impact microstructures in quartz is given by TEM studies. However, TEMs are not widely available, and sample preparation and handling is costly and time-consuming. Different methods, involving (3D) CL, (3D) EBSD and others on the cheaper and broader available SEM, are promising but not widespread yet (e.g. Bruijn, 2009). To date, the U-stage method has been the most commonly used technique.

Several examples of misinterpretations on impact and related structures are available in literature:

- PDF-like structures were reported and measured for volcanic ejecta from Toba, Indonesia (Carter et al., 1986). Many counter arguments and discussions followed (e.g. Alexopoulos et al., 1988; Parker and Toots, 1989 vs Grieve et al., 1989; Carter and Officer, 1989 vs Alexopoulos et al., 1989), until a TEM study (Goltrant, 1991) could not confirm the alleged PDFs.
- At Sevetin and Susice (Czech Republic), shock features in quartz were reported, that could later not be confirmed in a TEM study (Cordier et al., 1994)
- Numerous papers have been published on the Azuara structure in Northeast Spain, and heated discussions are ongoing between people and research groups for and against an impact hypothesis (e.g. Ernstson et al., 1985 vs Langenhorst and Deutsch, 1996; review of pro's and con's in Cortés et al., 2002). To date, the discussion has not ceased (e.g. Ernstson and Claudin, 2009)
- For summaries of various other structures where impact hypothesis is or has been discussed the reader is referred to review papers (Grieve et al., 1996; Reimold, 2007; French and Koeberl, 2010).

From the above, it should be clear that alternative methods of proving impact or shock metamorphism from quartz microstructures could be of great significance. As noted before, the main pitfall of using only U-stage techniques is that the a-axes of quartz can not be measured. Planes, for example PDFs, can be rotated in such a way their dip can be measured, relative to the c-axis. With the EBSD technique, both the position of the c-axis and the a-axes can be determined. However, in the SEM, the dip of a plane is not readily available without additional techniques, and only the strike of a plane is thus known. If the U-stage and EBSD data can be combined, they could be complementary, and thus give proof for the development of structures along certain crystallographic planes. U-stage and EBSD data have been combined previously for various types of research (e.g. Castro and Lagoeiro, 2009; Trepmann and Spray, 2006; Trepmann, 2008), but to current author's knowledge not in the same manner as here.

The goal of this thesis is therefore: To check the classical universal stage techniques for quantitatively confirming impact planar features in quartz, and to see whether the addition of Electron Backscatter Diffraction and/or Cathodo-luminescence data can provide more solid evidence.

It should be noted the focus lies on quantitative results, that is, proving the correspondence of planar features with distinct crystallographic planes by angular data. The following methods will be considered in this thesis:

1) The classical U-stage measurement technique, without indexing
2) The improved U-stage measurement technique, with indexing
3) The combination of U-stage and EBSD data
4) The addition of CL data, to see if it improves the result of method 3

Six different thin section samples from mostly accepted and confirmed impact sites are analysed, the sites being [examples of confirming TEM studies between brackets]: Ries, Germany [Goltrant et al., 1991; Vernooij and Langenhorst, 2005], Rochechouart, France [Trepmann, 2008] and Vredefort [Leroux et al., 1994]. 3 non-impact thin section samples are used for comparison, their origin being: Flinders Range, Australia, and the Ardennes, Belgium.

## 2. Methods

### *2.1. Used equipment and techniques*

#### *2.1.1. Thin section optical photography*

To prevent measuring grains more than once and to ensure the same grains were measured when combining different techniques, high resolution light microscope images of the used thin section samples were made in advance. High resolution flatbed scanner scans proved to be of too low quality for most samples. Therefore, the Leica DMRX light optical polarization microscope with camera at Utrecht University was used. Dependent on the sample, plane- or cross-polarized light was used. Using panorama photo stitching computer software (various software modules are available online), the separate photos were combined into one high resolution photograph of the sample.

#### *2.1.2. Universal stage*

The U-stage is a device that can be mounted on an optical light microscope. The stage has several axes of rotation, in addition to the microscope table itself – the only axis of rotation for a normal optical microscope. The additional axes increase observational power on a thin section to the third dimension, and allow quantification of optical and geometric features in the thin section. Included as an appendix is an extensive guide by the author on how to use the U-stage for measuring c-axes and poles to planar features in uniaxial crystals (e.g. quartz). The indicated method was followed for all samples, and measured grains were carefully indicated on the thin section photographs (note these photographs need to be rotated 180° to correspond with the view through the optical microscope; an effect of the lenses). The error on this U-stage data is approximately 5° (von Engelhardt and Bertsch, 1969; Ferrière et al., 2009). Some authors state lower errors of 1-2° (Bohor et al., 1987); a view not shared by current author based on the U-stage measurements performed for this thesis.

#### *2.1.3. Electron Backscatter Diffraction in the SEM*

EBSD analysis was performed using the Philips XL30S FEG SEM (Field Emission Gun Scanning Electron Microscope) at Utrecht University. For EBSD analysis, a sample is prepared for the electron microscope (the thin section is polished and coated), and emplaced in the sample chamber in a highly tilted manner (70°). In accordance with Braggs law for diffraction, some of the incoming electrons will be scattered off crystallographic planes in the sample, if present at the chosen position of measurement. From one plane or set of parallel planes, two "cones" of electron radiation will form. When these electrons hit a phosphor screen, they will light up as two parallel lines. The lines do not appear curved, since the angle of diffraction is so low for a crystalline solid, the radius of such cones is very large compared to the size of the phosphor screen. The lines that show up for a single (crystallographic) plane are called Kikuchi bands, and the pattern showing the representation of all interacting planes at the sampling position is called a Kikuchi pattern. Computer software, like the HKL Channel 5 software, indexes the Kikuchi pattern and recalculates it to an orientation of the crystal (e.g. quartz) relative to a reference orientation. For orientations, the error on the SEM-EBSD data is about 1-2°, although researchers need to bear in mind pattern misindexing (giving wrong orientations) may occur, dependent on sample, apparatus, and calibration quality. Figure 9 shows a simplified graphical representation of a typical EBSD installation. The above is a very short summary of extensive literature on EBSD and its applications, to which the reader is referred for more detailed descriptions (Randle, 1992; Schwarz et al., 2009).

For the samples studied in this thesis, different accelerating voltages and working distances were used to obtain the best EBSD pattern. The grains were selected via their position defined in the U-stage step, comparing the thin section photograph with the "live" SE (Secondary Electron, "topography"-related contrast of the sample) and FS (Fore Scatter, orientation contrast) images. Note that not all grains measured with the U-stage can

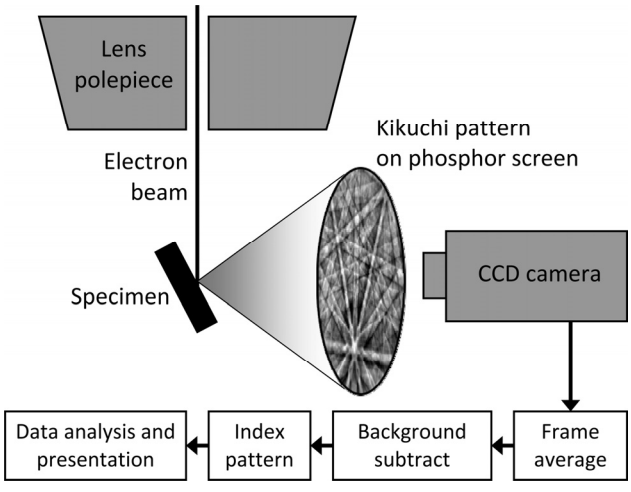


**Figure 9** Schematic diagram of a typical EBSD installation. Recreated after: Humphreys, 2001.

be measured by EBSD due to apparatus and time limitations, so the EBSD analysis can only be performed on a (random) selection of grains per sample. Most grains were covered using automatic beam mapping taking roughly between 100 and 2500 data points per grain.

*2.1.4. Cathodoluminescence*

CL analysis was performed on the FIB SEM at Utrecht University (the Focussed Ion Beam was not used in this research). Luminescence is the process in which the addition of energy gets an atom in an excited state, followed by the atom getting back in its unexcited state, by releasing the energy by emitting visible light. When the addition of energy occurs by electrons, for example in a SEM, this type of luminescence is termed Cathodoluminescence. The images made by CL display a contrast depending on composition – mainly by (heavy) metal contents – and defect concentrations (above after general summaries, e.g. Götze, 2004). PDFs may show up as distinct lines on these images. On the FIB SEM, it is also possible to insert colour filters before taking the CL image. Combination of the three grey-scale images as RGB images could give more information on PDF composition difference, and this colour CL might provide evidence for impact (M.F. Hamers, pers. comm., 2010). This method has not been applied in this thesis.

*2.2. Data processing*

*2.2.1. U-stage data*

As made clear in the appendix, the raw U-stage data is not directly suitable for use in a stereographic projection. Recalculation to a normal, "Silva compass" orientation represented in Clar's notation (dip direction/dip of pole, e.g. 273/15), was therefore performed as outlined there. Rotating the c-axis to the centre of the stereographic projection, as mentioned in the appendix, was also done by means of a formatted computer spreadsheet. This ensures all linked poles to planar features in the same grain are rotated in a similar manner, retaining the angular relations between them.

The simplest analysis on c-axis and poles to planar features data from the U-stage only involves the smallest acute angle between the c-axis and another pole. This angle can be measured in a stereographic projection, but it is also possible to calculate it by trigonometry after recalculating the angular data to Cartesian coordinates. Both can be done already with raw U-stage data. However, when the U-stage data is already corrected and the c-axis is rotated to the centre of a stereographic projection (i.e. the dip of the c-axis is 90°), the simplest method of obtaining the angle between the c-axis and another pole is: angle = 90° - dip of pole. The angles between the c-axes and the poles can now be plotted, in this thesis by a frequency distribution in 5° bins, as usually done for PDF data (e.g. von Engelhardt and Bertsch, 1969). See the results section or figure 8 for examples.

As mentioned in section 1.3.2, the improved (von Engelhardt and Bertsch, 1969; Stöffler and Langenhorst, 1994; Langenhorst, 2002; Ferrière et al., 2009; French and Koeberl., 2010) method of data processing for the U-stage measurements involves indexing of the angular data. To this end, a standard stereographic projection template with the c-axis centred and the impact-induced poles to planes (with 5° error circles) is used. The most modern version of this template, in correspondence to the planes in table 2, is shown in figure 10 (the New Standard Projection Template, or NSPT, of Ferrière et al., 2009). The c-axis centred U-stage data was plotted using the stereographic plotting software Stereo32, and placed on top of the NSPT in image manipulation software. In this way, a free rotation about the c-axis, hence the stereogram projection centre, could be performed to obtain a best fit of poles to planar features, by inspection according to the following criteria (roughly applied in this order):

1) Unindexable poles are assigned 0, equivocal (able to fit to multiple non-similar NSPT circles) are assigned X.
2) If two poles to planar features fall within the same NSPT circle, one of the two should be assigned 0. When multiple poles fall within multiple symmetrically equivalent NSPT circles, simply all should be counted (e.g. it is possible to have six poles assigned to plane {10-13}, as long as they fall in the six separate NSPT circles).
3) When a pole falls in an overlapping area, e.g. between {10-14} and {10-13}, it should be assigned to the closest centre.
4) As many poles as possible should be assigned to NSPT circles.
5) As many poles as possible should be as close as possible to the centre of the NSPT circle.
6) The best measurements (according to the U-stage measurements notes) should ideally fit NSPT circles best.

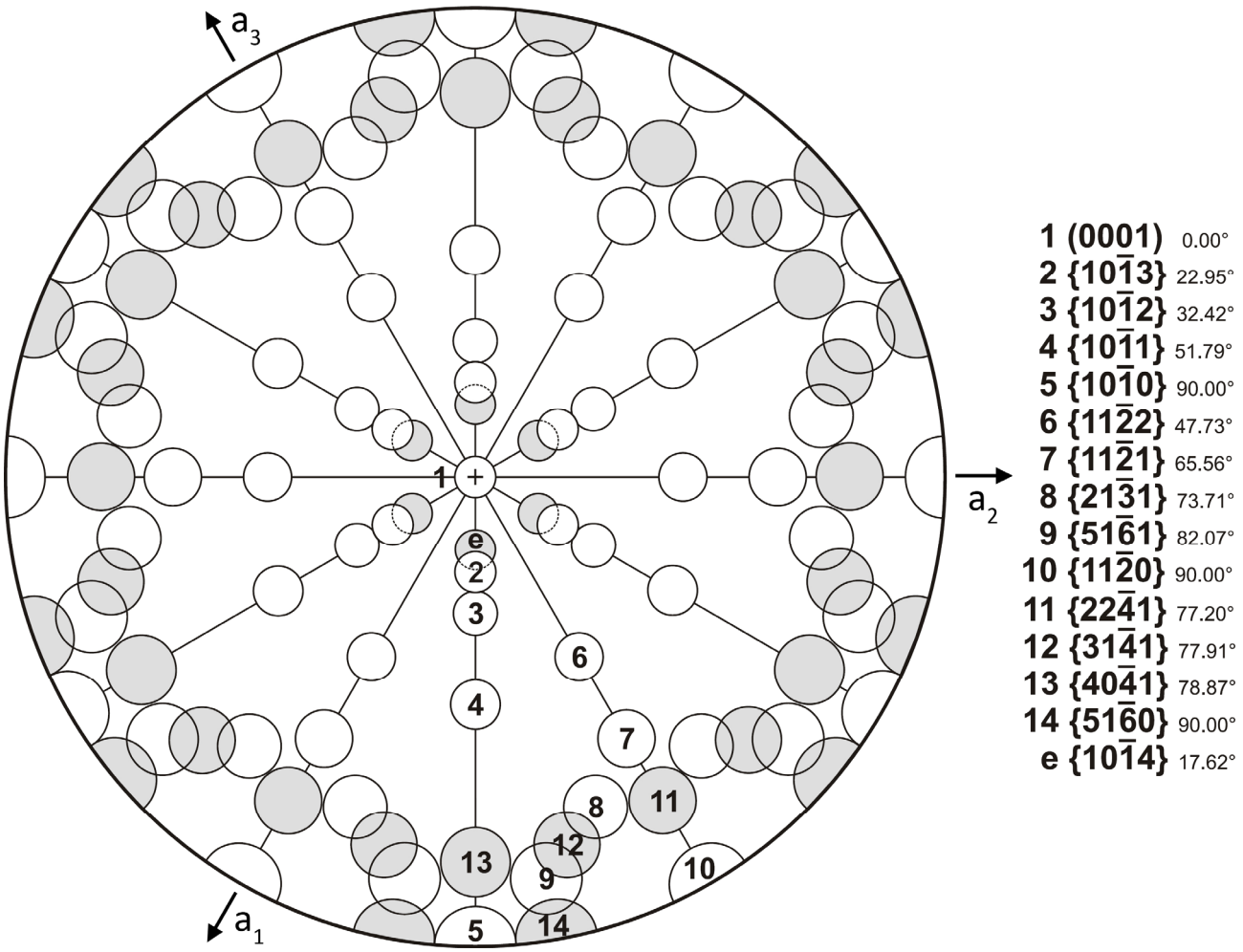


**Figure 10** New stereographic projection template (NSPT), used for indexing poles to PDF planes as measured with the U-stage. Each circle (5°) marks the position of the most common poles to PDF planes. Based on the standard stereographic projection of quartz with the c-axis centred, and the a-axes as indicated. Lower hemisphere, equal angle projection (Wulff-net). See text for discussion. From: Ferrière et al., 2009.

In most cases, the given criteria yield a single best result. This does not necessarily represent the truth, but only the best fit in an "empirical statistical" manner. After a best fit was found, the indexable planes were written down, keeping track of which index corresponds to which U-stage measurement. The main problem with the NSPT are grains with a single planar feature measured, as in many cases this yields an equivocal result (especially near the outer circle of the NSPT, where many planes with similar angles to the c-axis are present).

After indexing all grains in a sample, a frequency distribution plot can be made for all possible indexed planes. This can be represented on top of the binned angular data (examples shown in results section). As stated by Ferrière et al. (2009), to be able to compare different PDF orientation studies, it is important to indicate several parameters. In this thesis, the following is used:

- The frequencies are indicated in percentages, representing the so-called absolute frequency, i.e. $F_{hkil} = q_{hkil} / Q \cdot 100$ ($F_{hkil}$ = frequency, $q_{hkil}$ = number of sets belonging to a certain orientation or angle bin, Q = total number of measured sets) (von Engelhardt and Bertsch, 1969).
- Unindexed poles are included in the frequency calculations. In the figures, they are shown in the binned planar data as a different (lighter) grey-scale. They are not represented anymore in the indexed data, as they do not represent a specific plane.
- The number of measured grains and sets is indicated per plot, as well as the total percentage of unindexed poles.

It is noteworthy from a systematic study on obtaining and processing U-stage PDF data (Ferrière et al., 2009), the influence on the final data by an

unexperienced U-stage operator, as current author was, is only minor. Furthermore, measuring more sets per sample reduces the error on the data significantly (found by Ferrière et al. by comparing the result of the 20 first measurements to a set of 100 measurements on the same sample). Measuring over 100 sets is advised, mainly when the goal is to obtain shock barometry results. This is not the case for this study, so the minimum number of 59 sets (and usually more) per sample, due to time and sample constraints, should still give an adequate result.

*2.2.2. EBSD data*

By indexing the Kikuchi patterns, the EBSD acquisition software represents the orientation of the measured crystal relative to a reference state (for quartz, a crystal with the positive c-axis pointing upwards and the a-axes also fixed in a certain position). The difference in orientation is expressed by Euler angles, by which every orientation relative to a reference state can be represented as a series of three rotations. To this end, different conventions (rotation poles, rotation directions) exist. The HKL Channel 5 software uses a version of the Bunge convention, consecutively rotating counter clockwise about z, x' (the rotated x-axis) and z' (the rotated z-axis) as shown in figure 11.

From the Euler angles, it is possible to plot all crystallographic planes of the measured crystal, e.g. quartz. Using Channel 5's Mambo software module, this can be represented in a stereographic projection with chosen axes. The conventional manner is to plot relative to the flat-lying thin section, hence the positive z-axis centred and pointing upwards, and the x and y-axes at the edge of the projection (horizontal) according to the right-hand-rule for Cartesian coordinate systems.

For comparison with the U-stage data, it proves to be more convenient to be able to plot additional information in a stereographic projection. The full version of the stereographic projection software Stereo32 has the ability to import HKL Channel 5 Euler angle files. Unfortunately, Stereo32 only uses the {hkl} crystallographic system (Miller indices), instead of {hkil} (Miller-Bravais indices). To that end, for the possible crystallographic planes for PDFs, {hkil} was converted to {hkl} by simply discarding the "i" term (e.g. Stadelmann, 2010). Although the actual meaning of this transformation is not fully understood by current author (i.e. whether in the software this overlays a "pseudo-cubic" crystal structure upon quartz, or whether it is hexagonal {hkl} as it should be), thorough testing of this {hkl} conversion in both Stereo32 and Mambo showed exactly the same results for the planes as the {hkil} representation in Mambo. Furthermore, note that Stereo32 requires information on the axes of rotation (set by "EBSD origin transformation") as it uses slightly different conventions for Euler angles. Per sample, the origin transformation can best be found by trial and error, in comparison to the Mambo plots, as advised by one of the authors of Stereo32 (K. Röller, pers. comm., 2010).

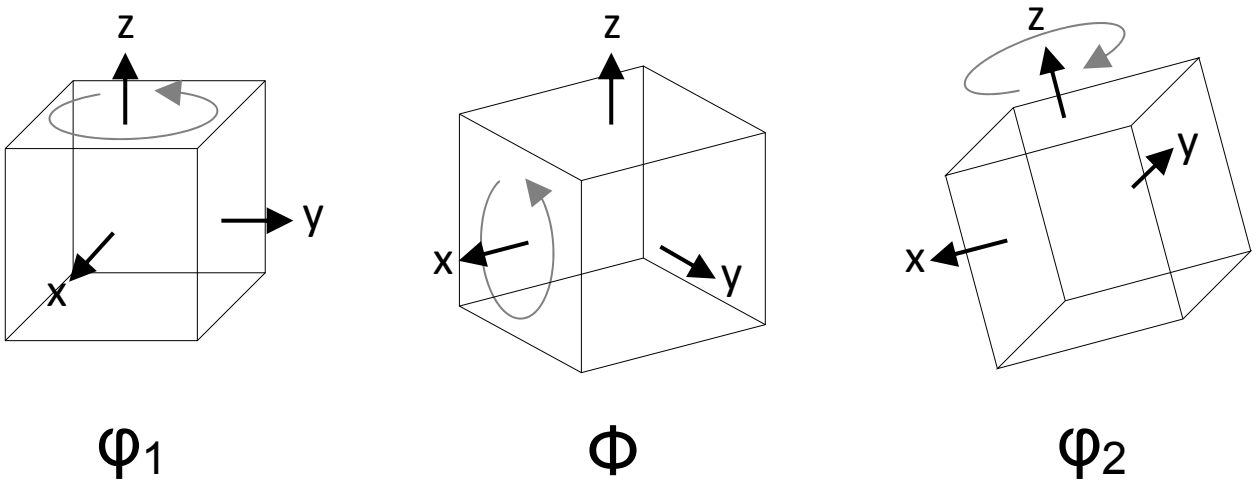


**Figure 11** Euler angles as used in the HKL Channel 5 software. 3 rotations are performed: $\phi_1$ about z, Φ about x', and $\phi_2$ about z'. In this manner, every orientation of the feature (in this thesis a quartz crystal, cubes shown for simplicity) can be expressed relative to the reference state shown in the first figure. All rotations are counterclockwise about the shown positive axes. The end situation (after rotating about z') is not shown. Recreated after: HKL Channel 5 Helpfile - Euler angles.

After finding the correct representation of the Euler angle data in Stereo32, the EBSD origin transformation was used to account for the 90° rotation between U-stage and EBSD data, resulting from how the sample is put in and how the x, y and z axes are defined (U-stage: sample flat and long side "North-South"; EBSD: sample flat, after tilt correction in the acquisition software, and long side "East-West". A schematic diagram explaining this difference is shown in figure 12). The rotation can be checked by comparing the U-stage and EBSD c-axes.

After the above correction, the U-stage data without the c-axis centred can be placed directly on top of the EBSD data. However, the EBSD data is made up of many data points and sometimes includes points clearly taken in an adjacent grain. To simplify re-indexing planar features using EBSD, the NSPT was fitted on top of the EBSD data using Stereo32 and the original Euler angle data. No change was made in the size of the error circles, as EBSD has a small error relative to U-stage data, and more overlap of different planes would only increase unclarity.

With the U-stage data on top of the rotated NSPT, re-indexing of the poles to planar features could be performed, called EBSD analysis 1. In this first analysis however, the slight misfit of the U-stage and EBSD c-axes sometimes proved to be problematic. The misfit is most likely caused by the error on the U-stage data and the positioning of the NSPT, reducing the scatter of the EBSD data (See for example figure 13a-d. In this particular example, the scatter on the EBSD data is rather small, but grains where the scatter of the EBSD data is larger than the NSPT circles have been observed). To check if indexing improved, the U-stage and EBSD c-axes were rotated to the same position, via the shortest route, hence along the shortest angle over the common plane between the two c-axes. For indexing, it proved most convenient to keep the U-stage data original (thus at the same position) and to rotate the NSPT. Grains for which the angle between the U-stage and EBSD data was >10° (little scatter in EBSD data) or >15° (more scatter in EBSD data) were discarded. Figure 13 shows an example of the stereographic projections corresponding to the steps explained above.

*2.2.3. CL data*

The contrast of CL images may show different or additional planes relative to the U-stage and other SEM imaging techniques. Comparison of the orientation of the CL images relative to the initial thin section photographs gives the rotation correction that needs to be performed first (the sample orientations differ). No dip data is available for the planes visible in CL, so only the strikes of apparent planar features can be measured the figures. These strikes are plotted on top of the EBSD and U-stage data. When the lines in CL indeed represent PDFs, the NSPT error circles should lie on the perpendicular line (passing through the stereographic projection centre) to the strike data. See figure 14 for an example.

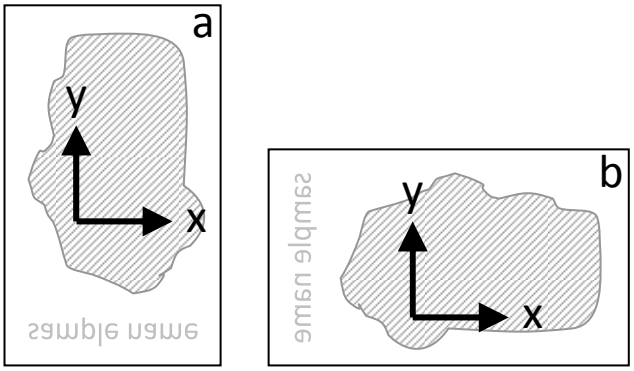


**Figure 12** Schematic diagram showing the different sample orientations and reference systems for the U-stage and the SEM. **a)** U-stage reference system, after corrections on U-stage data. The axes are defined corresponding to the orientation of the sample in the microscope. The z-axis points upwards, corresponding to the right-hand rule for Cartesian coordinate systems. The sample side (shaded grey) is of course up, the sample name is on the other side of the thin section (for the samples used in this thesis) **b)** SEM reference system (for EBSD after tilt correction). The reference system is similar to that of the U-stage, but rotated about the upward pointing z-axis. To compare U-stage and SEM data, a rotation correction of 90°or 270° thus has to be performed, dependent on the precise sample orientation (samples may be rotated 180° in the U-stage and/or the SEM)

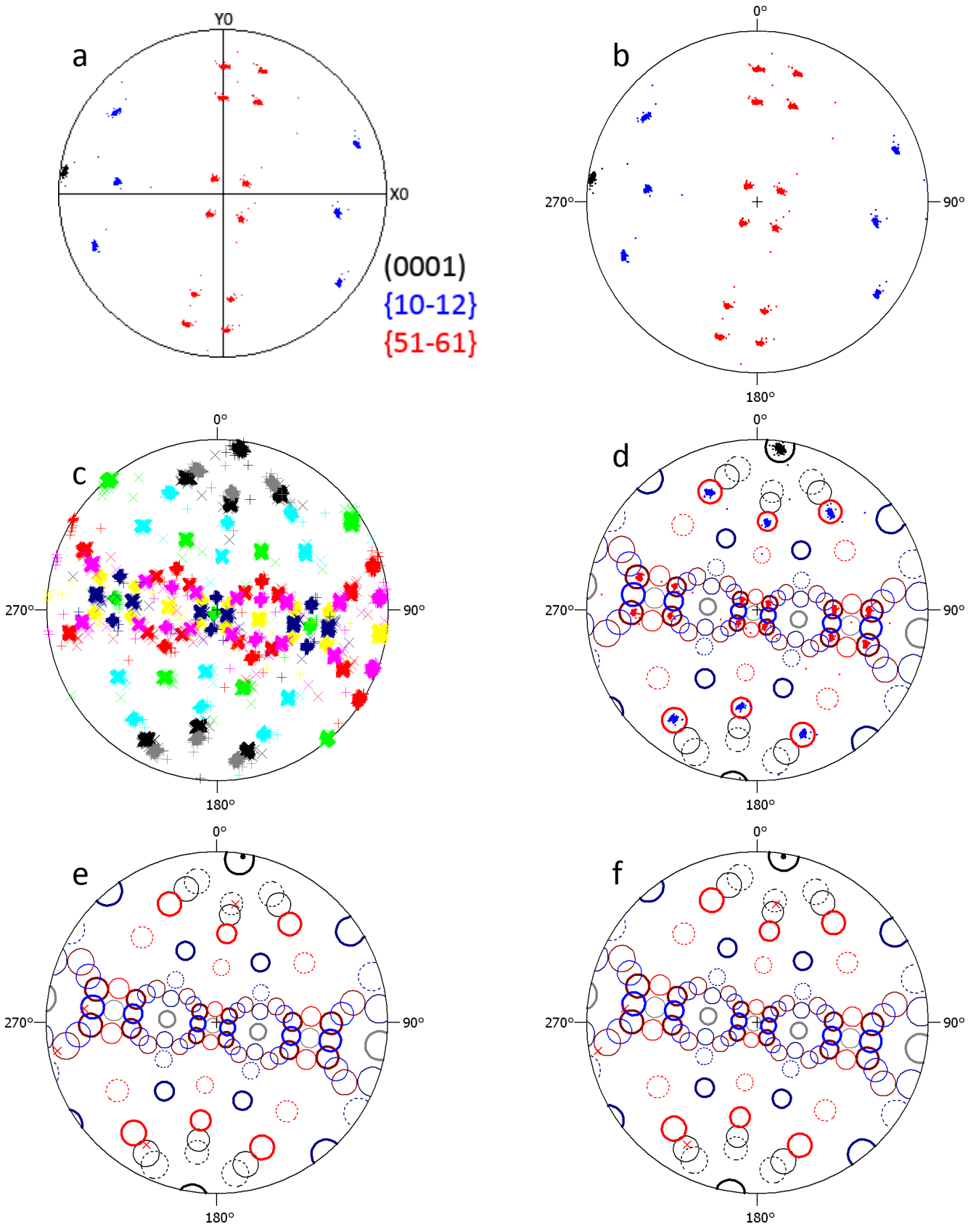


**Figure 13** Steps in processing the EBSD data. **a)** HKL Channel5 Mambo equal area, lower hemisphere plot of some poles to PDF planes, from the EBSD data. The presence of multiple poles (6 for {10-12}, 12 for {51-61} is related to the presence of symmetrically equivalent planes, and possibly Dauphiné twinning (twins in a quartz crystal, 60° rotated about the c-axis; Trepmann and Spray, 2006) **b)** Stereo32 equal area, lower hemisphere plot of some poles to PDF planes. A correct setup of Stereo32 thus yields the same results as a. **c)** Stereo32 equal angle, lower hemisphere plot of all 15 possible poles to PDF planes. It should be evident this representation is not really workable in further analysis, especially for samples with more scattered EBSD data or by accident multiple measured grains. Note the change in projection relative to a and b (easier for analysis), and the 90° rotation to fit the U-stage data. **d)** Stereo32 equal angle, lower hemisphere plot of the NSPT fitted (by using the average Euler angles) to some poles to PDFs from the EBSD data. This representation thus again shows all possible orientations for poles to PDFs (like c), but is easier in analysis. **e)** Stereo32 equal angle, lower hemisphere plot of the NSPT, combined with U-stage data. Black dot = U-stage c-axis, Red crosses = U-stage poles to planar feature measurements. Indexing the poles to planar features is now possible (termed EBSD analysis 1). The EBSD vs U-stage c-axis misfit is quite small for this particular sample, but can be larger for other samples (e.g. the black dot lies outside the black circle). **f)** Stereo32 equal angle, lower hemisphere plot of the NSPT, combined with U-stage data. Relative to figure e, the NSPT has been rotated via the common plane between the U-stage and EBSD c-axes. The U-stage poles to planar features can now be re-indexed again (termed EBSD analysis 2).

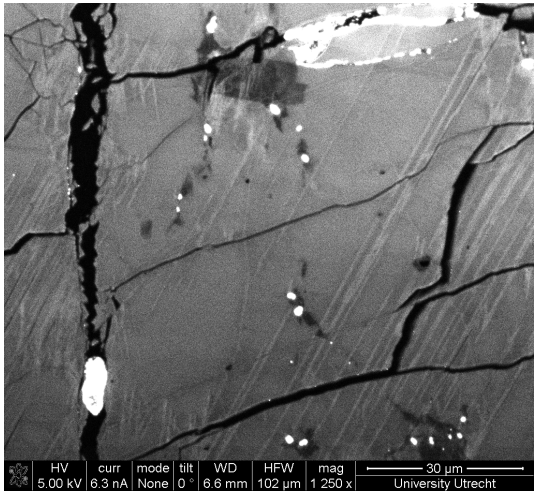


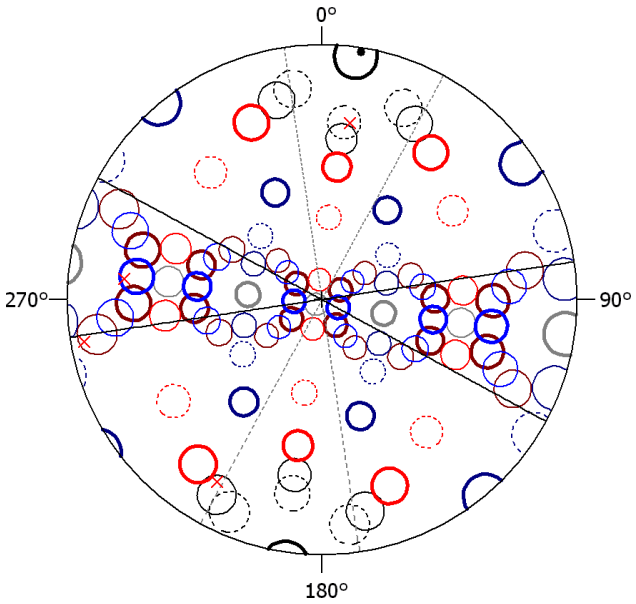


**Figure 14** CL image and expression of observed planes on top of the stereographic projection of figure 13e. The black solid lines represent the strikes of the planes observed in the CL image, the grey dashed lines the orthogonals to the black lines, on which PDFs should lie. Normally, the black solid lines should directly fit the strikes observed in the CL image, but due to the 90° rotation between U-stage and SEM sample orientation, the grey dashed lines match now. Note multiple NSPT circles (hence PDFs) could fit the grey dashed lines. In this example, one U-stage measured PDF seems to fit the CL data, 3 do not, and 1 CL measurement does not fit any U-stage data.

**Table 4** Analysed samples

| Sample | Location | Rock type | Impact age (Ma)* | U-stage measurements | | | | | | SEM analyses | |
|---|---|---|---|---|---|---|---|---|---|---|---|
| | | | | Measured Main, (Minor) | # Grains | # Sets | Avg. # Sets/Grain | Max. # Sets/Grain | % Unindexed | EBSD | CL |
| RI-37 | Aumühle quarry, (Ries), Germany | Crater floor granite fragment | 15.1 ±0.1 | PDFs, (PFs) | 85 | 214 | 2.52 | 6 | 5.6 | YES | YES |
| RI-43 | Polsingen (Ries), Germany | Basement fragment in melt sheet | 15.1 ±0.1 | PDFs, (PFs) | 51 | 140 | 2.75 | 7 | 15.0 | x | x |
| RI-47 | Polsingen (Ries), Germany | Basement fragment in melt sheet | 15.1 ±0.1 | PDFs, (PFs) | 50 | 137 | 2.74 | 6 | 13.1 | x | x |
| OTT-2 | Otting (Ries), Germany | Suevite | 15.1 ±0.1 | PDFs, (PFs) | 37 | 90 | 2.43 | 4 | 13.3 | x | x |
| MRO-5 | Montoume quarry (Rochechouart), France | Rochechouart-type lithic breccia | 214 ±8 | PDFs, (PFs) | 51 | 94 | 1.84 | 4 | 7.5 | x | x |
| H4 | Vredefort, South-Africa | Granite fragment | 2023 ±4 | PDFs, PFs | 66 | 69 | 1.05 | 2 | 15.9 | x | x |
| SAPP2 | Flinders range, Australia | Quartzite | N/A | DL, (inclusion trails) | 50 | 61 | 1.22 | 2 | 26.2 | YES | x |
| SARB2 | Flinders range, Australia | Quartzite | N/A | DL, (inclusion trails) | 50 | 65 | 1.30 | 2 | 26.2 | x | x |
| B14 | Ardennes, Belgium | Quartzite | N/A | DL, (inclusion trails) | 50 | 59 | 1.18 | 2 | 22.0 | x | x |

*Earth Impact Database, 2010

## 3. Results

### *3.1. Samples*

A total of nine samples was investigated in this study. Six of these samples are from three different confirmed impact sites, and three from two non-impact related normal deformational settings. The characteristics and taken measurements are summarized in table 4.

### *3.2. U-stage analysis*

Figures 15 and 16 show the classical binned representation of angles between poles to planar features and the c-axis, together with the indexed form, on the same scale. The indexed form should be regarded as a single position, so unlike the binned data, the "width" of the indexed data in the graph is for display purposes only. As noted previously, the sets that could not be indexed are indicated in the binned data as a light-grey colour, per angular domain. Therefore, the total of each dark + light-grey bin represents the actual classical binned way of display (all measured sets included). The unindexed sets are not visible anymore in the indexed data in the graphs. In summary, all bins per graph together add up to 100%, while the indexed bars will add up to 100% - % unindexed.

The following should be noted in the analysis of the figures:

- The most frequently indexed planes are, as mentioned in previous sections, planes {10-13}, {10-12} and (0001). Plane {10-14} is also abundant, but as it has only recently been added (Ferrière et al., 2009), its abundance has not previously been noted. Bear in mind many of the measurements now assigned to plane {10-14} could have been assigned to plane {10-13} if plane {10-14} was not present in the NSPT, due to their overlap.
- The Vredefort H4 impact sample is the clearest exception, as it almost exclusively indexes as plane (0001). It has been noted before that due to the age of the Vredefort structure, no actual PDFs have survived post-shock annealing, but only basal Brazil twins (Leroux et al., 1994). Brazil twins may be visible with the optical microscope when they are decorated, but some of the measured planes could also represent PFs.

The difference between impact and non-impact samples is small, but the comparison can be summarized as follows (from table 4, figure 15, figure 16):

- Usually a lower number of sets per grain for the non-impact samples, although the Vredefort H4 impact sample (figure 15c) shows a clear exception to this.
- Slightly more higher angles (>30°) in the binned angular data for non-impact samples.
- No distinct bell-shapes in the binned angular data for non-impact samples. Non-impact sample SARB2 (figure 16b) comes closest to a bell shape.
- Similar planes indexed for impact and non-impact samples.
- A somewhat higher non-indexing rate for non-impact samples.

### *3.3. EBSD analysis*

The EBSD analysis as outlined in the sections 2.1.3 and 2.2.2 has been performed on impact-sample RI37 and non-impact sample SAPP2. Figures 17 and 18 show the results of the combined EBSD and U-stage data. Both analysis 1 (non-corresponding c-axes) and analysis 2 (corresponding c-axes by rotation of EBSD data over shortest angle) are shown. The displayed indexed U-stage data is shown for comparison. It differs from figures 15 and 16 by only taking into account the grains analysed using EBSD.

A comparison of the graphs shows the non-indexing rates increase due to the addition of EBSD data. This can be expected, as basically the same analysis is performed on more data. Note it is impossible for non-indexing rates to decrease due to the addition of EBSD data. Furthermore, indexing rates are slightly better for EBSD analysis 2. The most striking result is however the indexing rate for the non-impact sample: almost all planes that were indexed after the U-stage analysis alone, could not be indexed anymore after addition of EBSD data.

The misfit with the U-stage indexing (for the EBSD analysed grains only) includes previously equivocal grains (indexed as X), new and old unindexed grains (indexed as 0), different fits in overlapping areas (e.g. plane {10-14} vs. plane {10-13}) and other different fits. The misfits are as follows: RI37 EBSD analysis 1: 48.7%; RI37 EBSD analysis 2: 26.9%; SAPP2 EBSD analysis 1 and 2: both 71.9%. The decreased misfit for RI37 EBSD analysis 2 is as expected, as no misfits should ideally be introduced now by the non-correspondence of the U-stage and EBSD c-axes, but part of the non-indexing rate of 18.0% is still included. The high misfit rates for the SAPP2 analyses are of course (only) inherent to the high non-indexing rates.

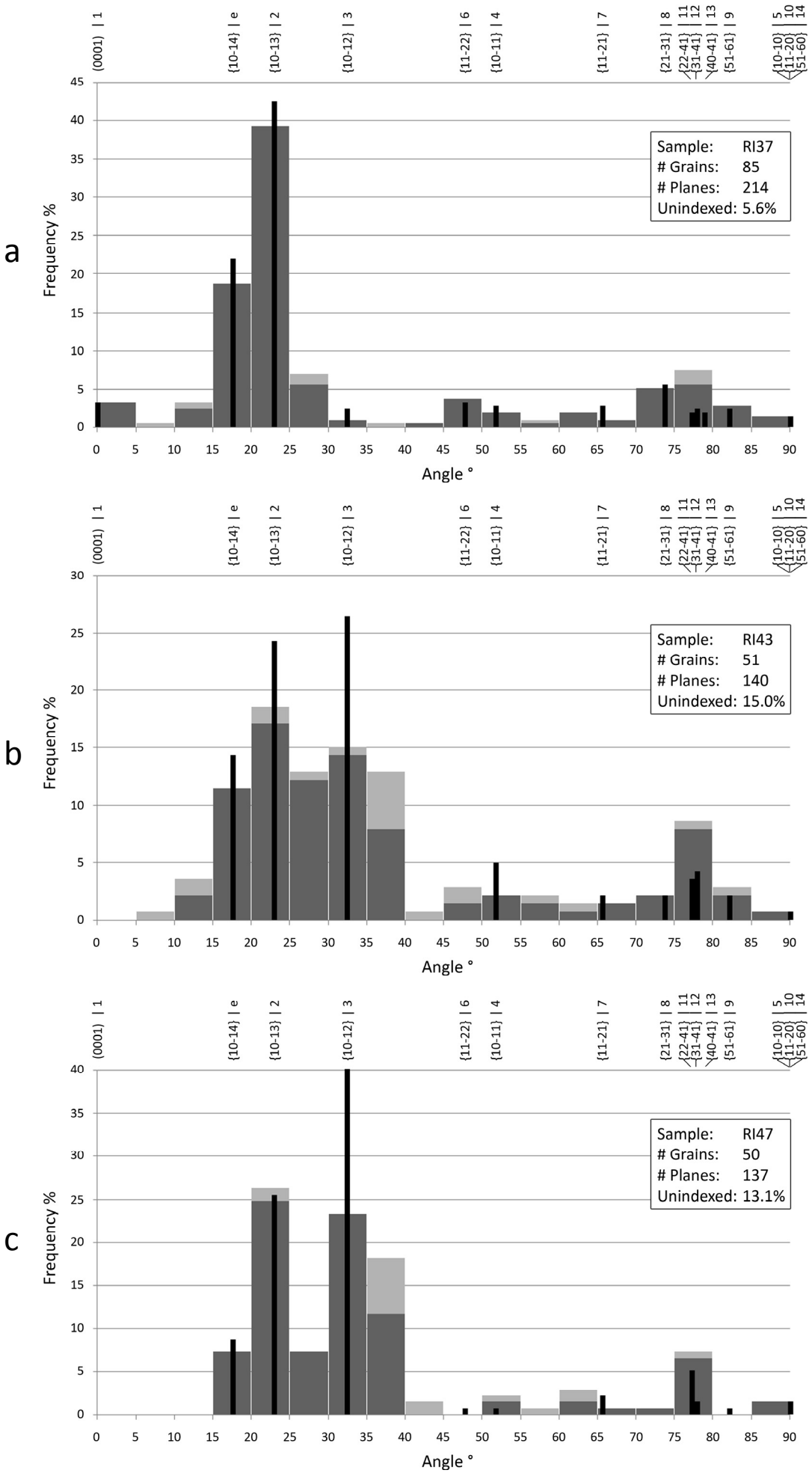


**Figure 15** Frequency distribution plots of impact produced planar features (mainly PDFs, some PFs) in quartz grains. The binned angular data shows the frequency distribution of the polar angle (the angle between the quartz c-axis and the pole to the planar feature). Dark grey bins: indexed angles; Light grey bins: non-indexed angles. The black "spikes" show the frequency of indexed planes (indicated above) using the NSPT. See text for details and discussion.

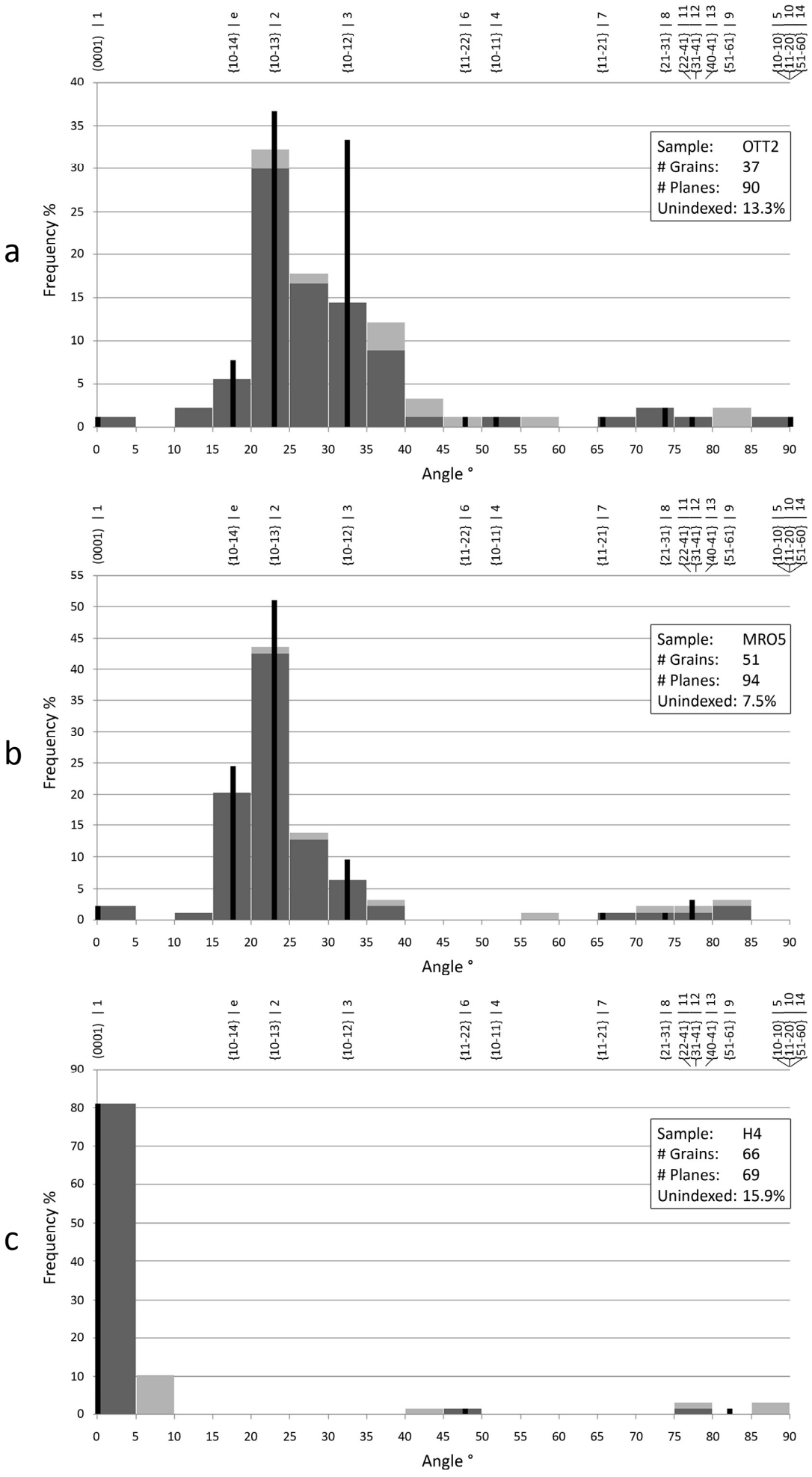


**Figure 15 (continued)** Frequency distribution plots of impact produced planar features (mainly PDFs, some PFs) in quartz grains. The binned angular data shows the frequency distribution of the polar angle (the angle between the quartz c-axis and the pole to the planar feature). Dark grey bins: indexed angles; Light grey bins: non-indexed angles. The black "spikes" show the frequency of indexed planes (indicated above) using the NSPT. See text for details discussion.

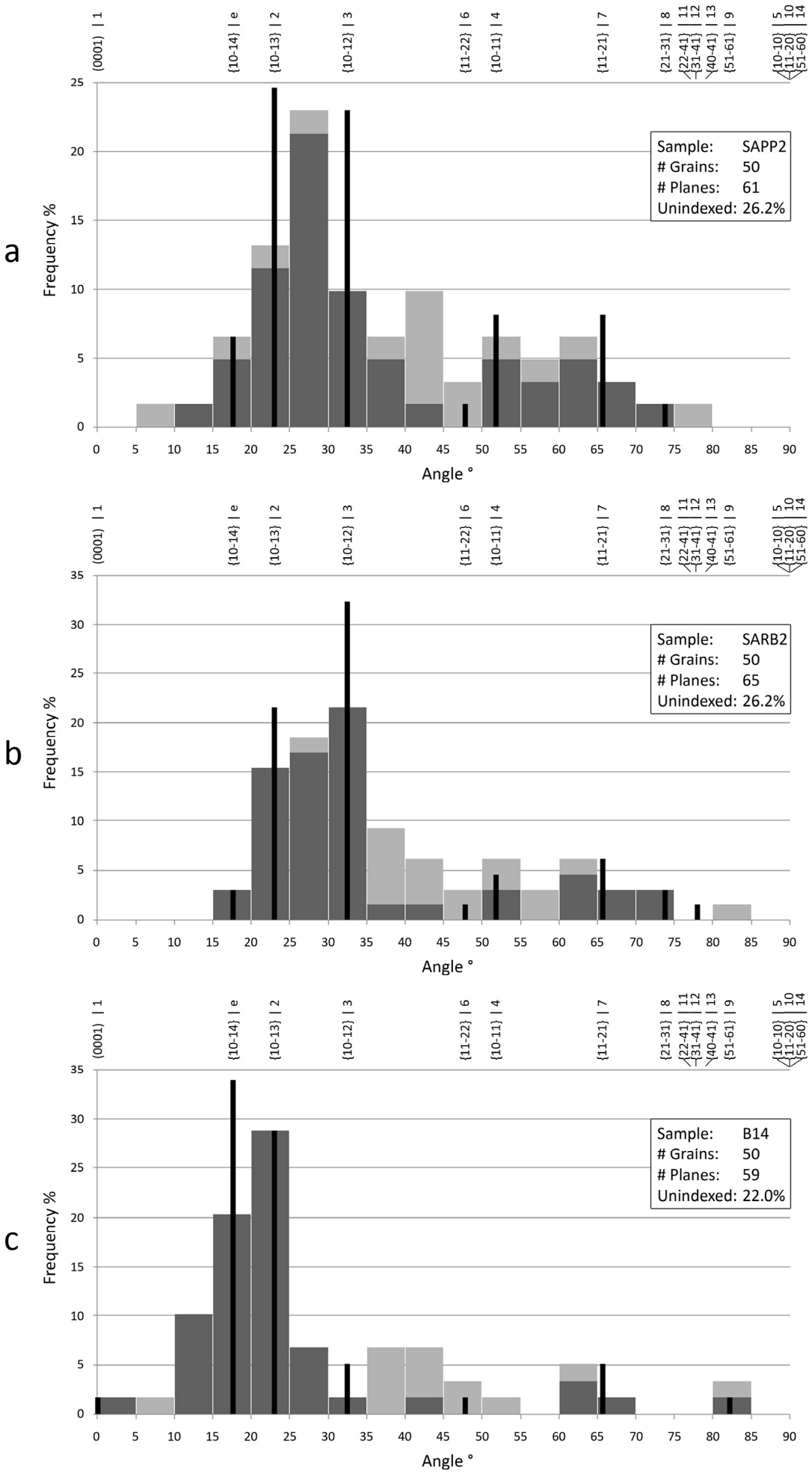


**Figure 16** Frequency distribution plots of non-impact produced planar features (mainly DL, some inclusion trails) in quartz grains. Further description as for figure 15. See text for details and discussion.

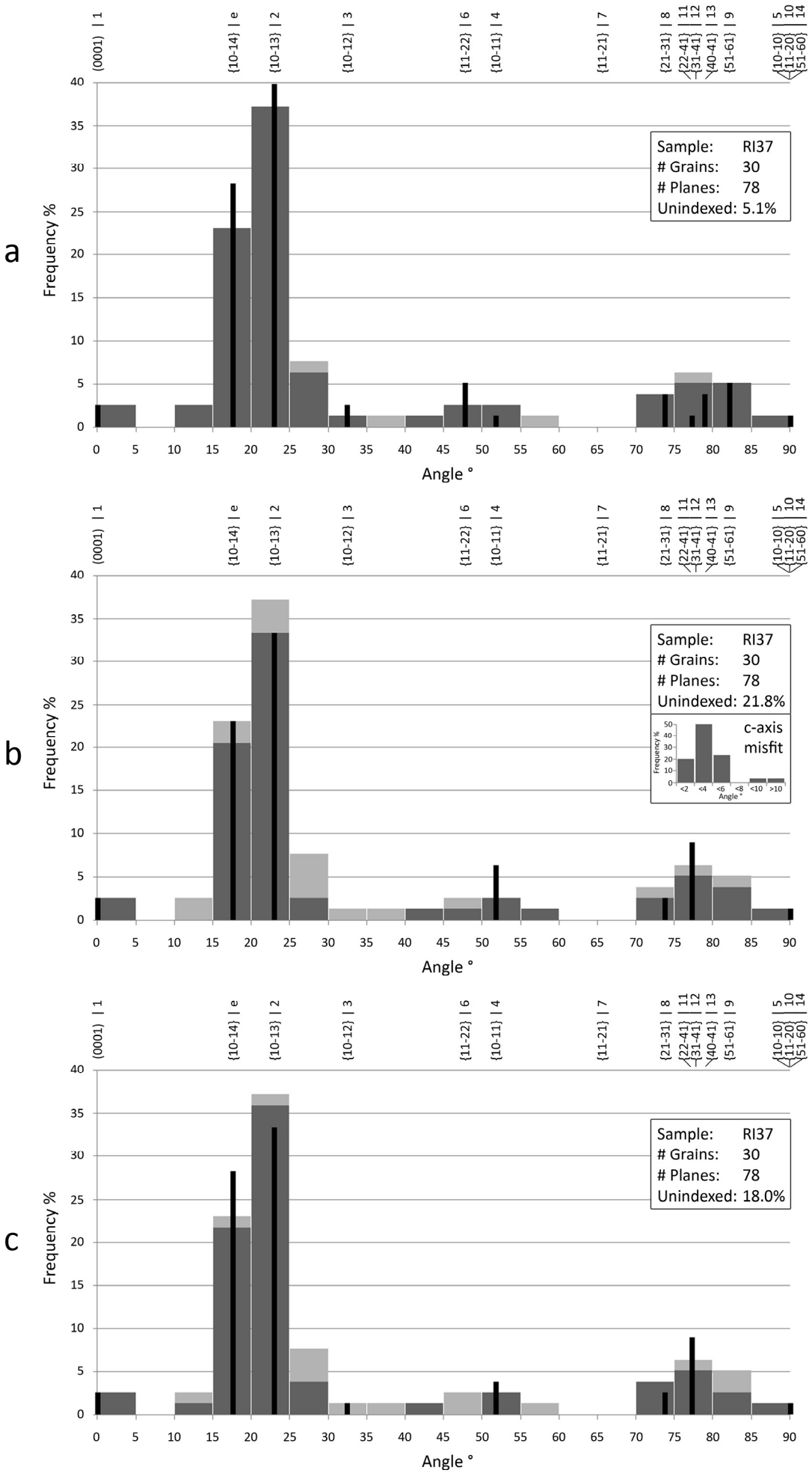


**Figure 17** Frequency distribution plots of impact produced planar features (mainly PDFs, some PFs) in quartz grains. Further description as for figure 15. **a)** Replotted U-stage only data for the grains analysed with EBSD. **b)** EBSD analysis 1. Small inset shows the misfit of EBSD and U-stage c-axes. **c)** EBSD analysis 2. See text for details and discussion.

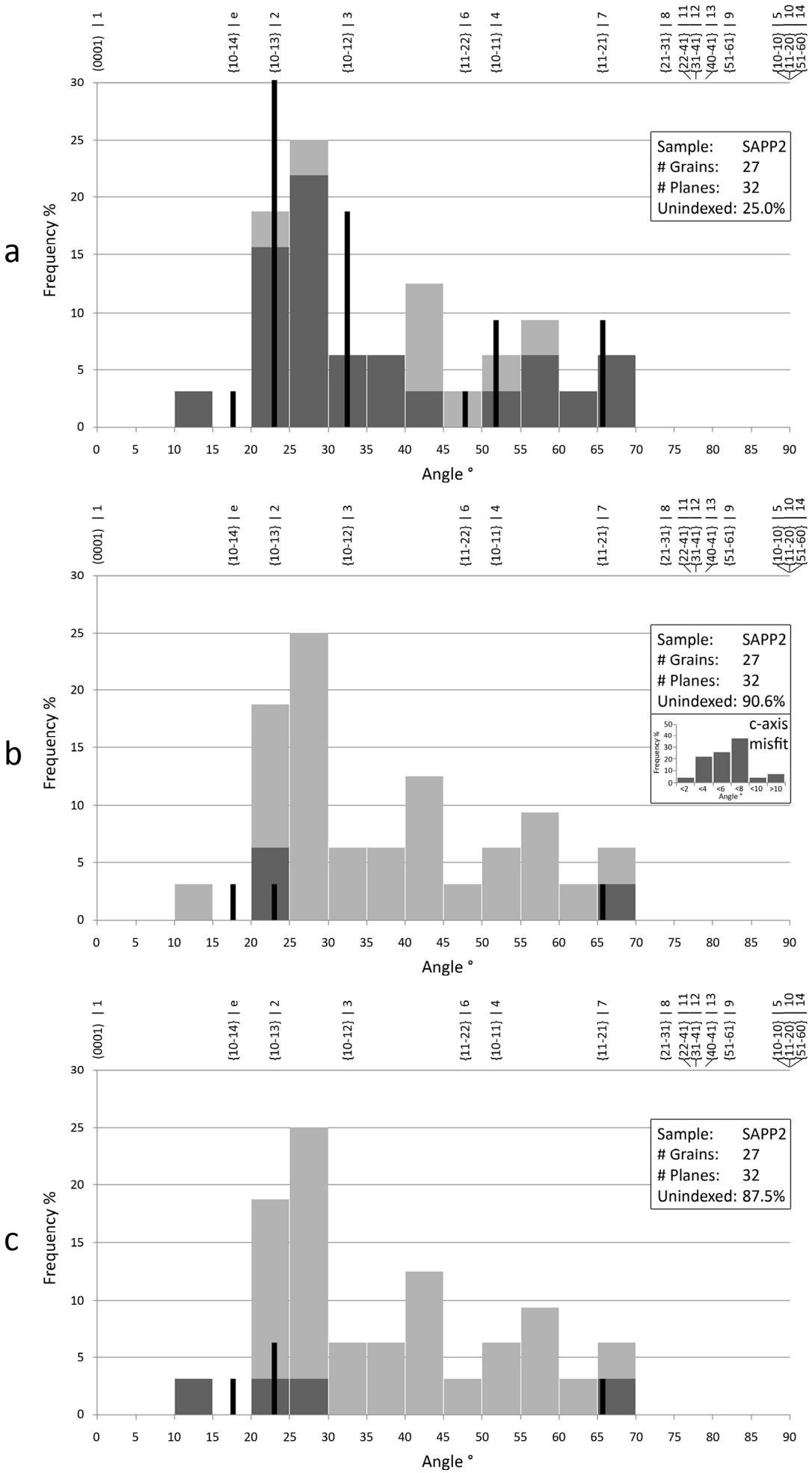


**Figure 18** Frequency distribution plots of non-impact produced planar features (mainly DL, some inclusion trails) in quartz grains. Further description as for figure 15. **a)** Replotted U-stage only data for the grains analysed with EBSD. **b)** EBSD analysis 1. Small inset shows the misfit of EBSD and U-stage c-axes. **c)** EBSD analysis 2. See text for details and discussion.

*3.4. CL Analysis*

The CL analysis has only been performed on sample RI37, on grains also analysed using EBSD. Figure 19 shows several examples of the representation of CL images in a stereogram, combined with EBSD analysis 1. It should be clear multiple different PDFs could result in the same strike in the stereogram. In quite some cases, the CL data fits (some) of the added U-stage data. However, if measurements using the CL images do not fit U-stage data, this does not directly mean a misfit: the PDFs could for example not be visible or were not noted with the optical microscope, and vice versa. Furthermore, some observed planar features in the U-stage might actually not be PFs or PDFs, and are therefore not visible with CL, but this is difficult to check without a new (time-consuming) U-stage analysis.

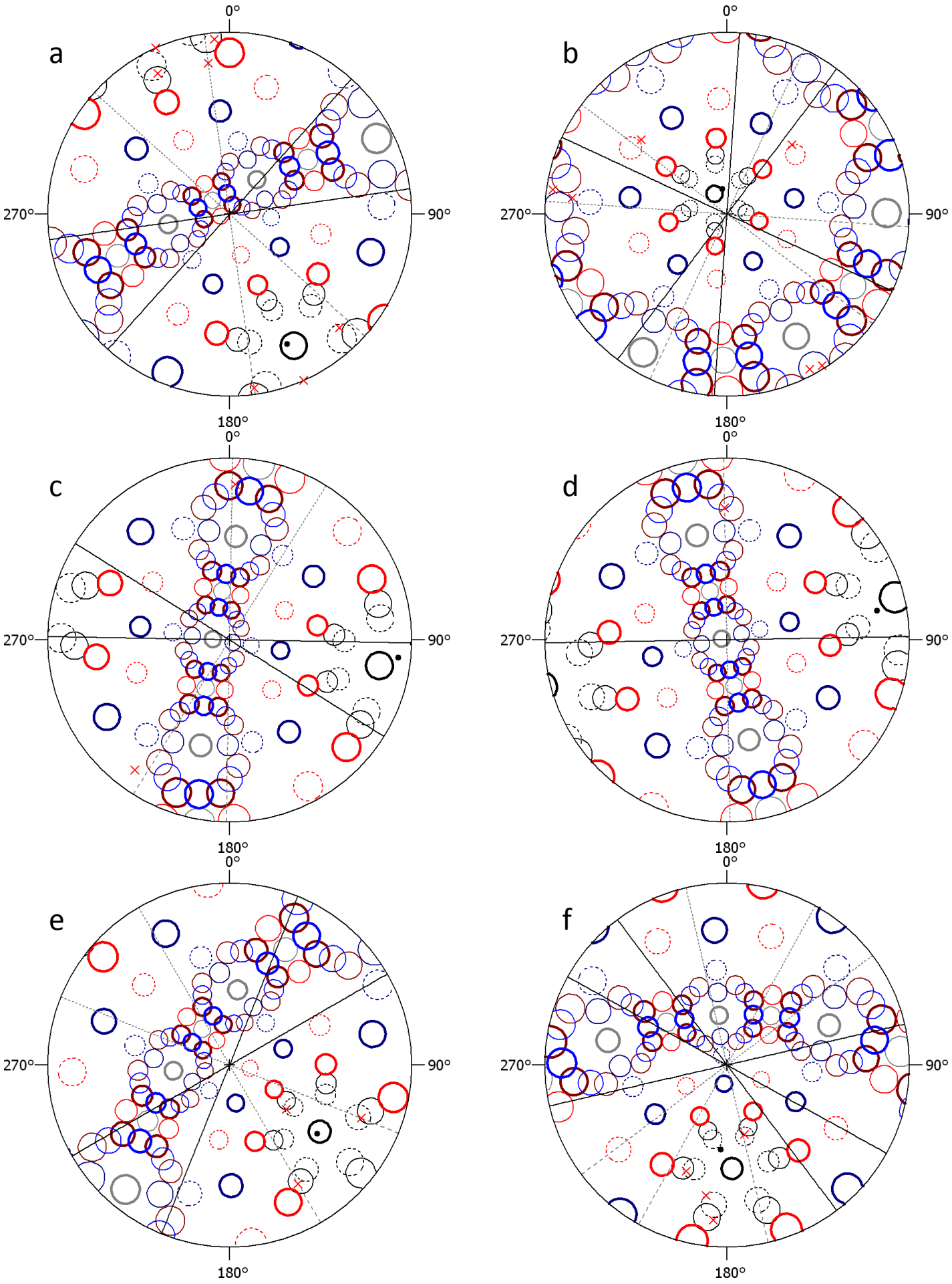


**Figure 19** Examples of strikes measured in CL images, superposed on EBSD analysis 1 stereographic projections, for grains in sample RI37. See figure 14 for description of the method and the legend. **a)** Grain 01: 6 U-stage planes, 2 out of 2 CL planes match. **b)** Grain 12: 6 U-stage planes, 2 out of 3 CL planes match. **c)** Grain 14: 2 U-stage planes, 2 out of 2 CL planes match. **d)** Grain 15: 1 U-stage plane, 1 out of 1 CL planes match. **e)** Grain 21: 3 U-stage planes, 2 out of 2 CL planes match. **f)** Grain 22: 4 U-stage planes, 1 out of 3 CL planes match. See text for discussion.

## 4. Discussion

### *4.1. U-stage analysis*

In the analysis of the U-stage data two previously applied methods were used to confirm an impact origin for the quartz microstructures: binned data of the angle between the c-axis and the poles to planar features in a grain, and so-called indexed data. These methods were used to see if their application can indeed unequivocally confirm shock metamorphism. For the investigated samples, the current author's opinion is they can not. For example, the impact sample Vredefort H4, although quite different from the other impact samples, shows the amount of sets per grain is not always distinctive for impact samples relative to non-impact samples. Furthermore, although the non-impact samples generally show some more higher-angle measurements, the difference between e.g. RI43 (impact) and SARB2 (non-impact) is minute, and non-impact samples SAPP2 and B14 show "spikes" in their angular data that according to previously used criteria by other authors (see section 1.3.2, figure 8, and later comments) could indicate impact origin. Indexing of the U-stage data does not provide conclusive criteria as well, as it results in similar planes for all samples. Although the non-indexing rate is higher for non-impact samples, the difference is not very large (e.g. 22.0% for B14 vs. 15.9% for H4), and can easily be nullified by poorer measurements or harder to measure samples. Also bear in mind all samples studied here are of known impact or non-impact origin. So, even with this prior knowledge, no distinct quantitative criteria can be set up, let alone distinction can be made without knowing the origin in advance. In fact, the plots for the non-impact samples of this thesis could even be used as "evidence" for impact, according to the previous literature!

Note the main goal of the U-stage measurements was to check the differences between impact and non-impact samples in a quantitative way. For the impact samples, mainly planar features corresponding to the description of PDFs and PFs (section 1.2.3.2) were measured. For the non-impact samples however, basically all planes were measured. Using the qualitative criteria for the optical microscope from section 1.3.1, many of these planes were clearly DL, apart from a few planes that resemble PDFs. Therefore, when someone were to measure the used samples without knowing their origin yet, the non-impact samples could easily be picked out in a qualitative manner. It is emphasised however again that many of the past discussions on impact versus non-impact origin could not be solved by a qualitative approach using only light microscopy. This justifies the approach taken in this thesis, although it would have been interesting to include less obvious non-impact samples in this study.

Some remarks can be made regarding previously published literature. First, note figure 8 is strange in a sense that the non-impact histogram is shown in different binned intervals compared to the impact histograms. More importantly, the non-impact graph is based on much more (compiled) data than the impact histograms. The figure is based on older compilations (Carter, 1965; Carter and Friedman, 1965; Hansen and Borg, 1962) that show similar bell-shaped characteristics, and so do some of the original single-sample graphs (Fairbairn, 1941; Ingerson and Tuttle, 1945). However, the compilation is also based on original single-sample data as shown in figure 20 (Christie and Raleigh, 1959) that does not show a bell-curve! This is an important observation as it could have been recognised from relatively old literature already U-stage work alone is insufficient in proving impact. Unfortunately, the compilation (figure 8) of Carter (1965) has been used in later literature a lot, while it proves to be misleading in suggesting a bell-curve should be observed for DL samples.

Another interesting literature example comes from the previously mentioned discussion on the Azuara structure in Spain. Different observations have been used to (dis)prove an impact origin for this structure. Of course, U-stage measurements have been taken on planar elements in the samples. Figure 21 shows binned angular data for samples from the Azuara structure. It is argued this data can provide evidence for impact (Ernstson et al., 1985). Similar results have been obtained for other samples from the structure as well (summarised by Ernstson and Claudin, 2009). It should be clear figure 21 is as good or as bad as the results shown in this thesis. An impact origin for the Azuara structure can thus not be (dis)proved with the U-stage method alone. The Azuara structure, being subject of an ongoing debate on its origin, is therefore an illustration on where the outcome of this thesis can be used for future research.

Conclusively, the results for the samples considered in this thesis are not in line with criteria from previous research. Unless confirmed by e.g. a TEM

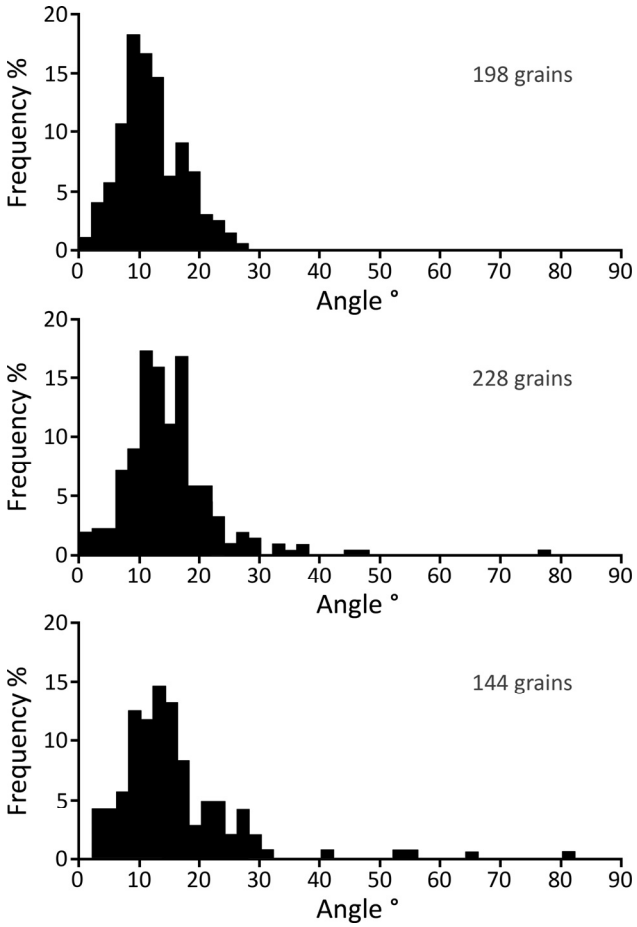


◄**Figure 20** Histograms of orientations of non-impact planar microdeformation features (DL) in quartz grains, showing the frequency distribution of the polar angle (the angle between the quartz c-axis and the pole to the planar feature). Samples are from the Orocopia Mountains, Southern California). Data from these graphs is included in the composite graph for non-impact samples of figure 8. Note the graphs do not display a clear wide "bell-shape" (used as evidence for non-impact), but have distinct peaks (used as evidence for impact). See text for discussion. Recreated after Christie and Raleigh, 1959.

▼**Figure 21** Histogram of orientations of planar microdeformation features in quartz grains from the Azuara structure, Spain, showing the frequency distribution of the polar angle (the angle between the quartz c-axis and the pole to the planar feature). The peak-like nature of this graph (implied parallelism to certain crystallographic planes in quartz) has been argued to present evidence for impact, but this has been debated thoroughly. See text for discussion. Recreated after Ernstson et al., 1985.

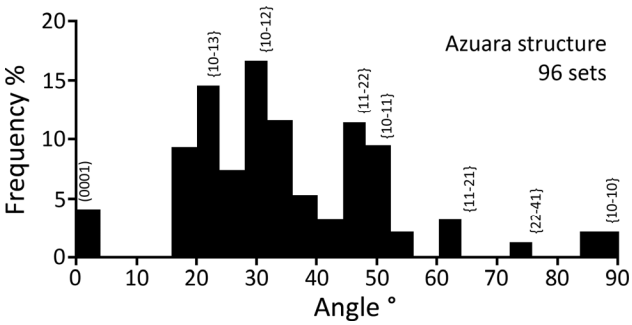


study or supported by qualitative data (in a critical manner, both on the micro- and macroscale), U-stage measurements do not seem sufficient to definitively prove impact. It has been acknowledged in such words multiple lines of evidence together with U-stage data are important (e.g. Vernooij and Langenhorst, 2005). In many cases however, there seems to be a focus on U-stage measurements as an almost unequivocal proof (e.g. Stöffler and Langenhorst, 1994; Ferrière et al., 2009).

*4.2. EBSD analysis*

The clear advantage of EBSD relative to the optical microscope is that the orientation of a quartz crystal can be determined, including the three a-axes. Due to symmetry, the actual distinction between these axes can not be made, so the resulting orientation is still 3-fold symmetric. This is not of influence on indexing PDFs. A clear disadvantage of normal EBSD is no 3D data can be obtained on planar features in the sample. This information has to come from a different source: in this case, the data was combined with the U-stage data to see whether this could unequivocally confirm the presence of structures parallel to certain crystallographic planes in quartz, hence shock metamorphism. The addition of EBSD data provides a clear distinction between impact and non-impact samples. As noted in section 3.3, almost none of the U-stage only indexed PDF planes could be confirmed in the non-impact sample, whereas in the impact sample, much more PDF planes could be either confirmed or were found to be corresponding to other PDF planes.

The initial manner of combining the U-stage and EBSD data, analysis 1, allows simple pasting of the data on top of each other, keeping in mind the U-stage and EBSD sample positions are 90° rotated. A more critical note should be made regarding analysis 2. This method gives better indexing rates as the U-stage and EBSD c-axes are set equal. In this thesis, the EBSD data was rotated over the common plane between the two c-axes. Probably, the statistical meaning of such a rotation should be tested to conclude whether it is valid. This should account for the errors on both the U-stage and EBSD data, and the scatter in the EBSD measurements, as sometimes observed but not used anymore in a later stage for simplicity (by the fitting of the NSPT on top of the EBSD data). Such a check has not been performed yet, also since analysis 1 already shows a clear distinction between impact and non-impact data; at least for these two samples.

*4.3. CL analysis*

The CL data was used to see if more PDFs could be resolved than with other methods. It has only been applied on impact sample RI37. As clear from section 3.4, many PDFs are indeed clearly visible in CL images. However, as dip data is not available, CL data is usually equivocal in the PDF planes that could be assigned to the strike of visible planar features. Correspondence to U-stage data does not prove anything as well, as in both ways, features could be visible in one apparatus and not in the other. The only use of CL data could be to go back to the U-stage and check if more sets could be resolved by the knowledge of more PDF strikes, or to critically evaluate U-stage measured planes that could not be observed by CL. However, this is time consuming, and probably gives only minor additional results, if any at all. Conclusively, CL data as taken here is not useful in a quantitative manner. It could be of importance for a more qualitative distinction of PDFs, i.e. in their comparison to DL by first visual appearance, and so can colour CL. A more quantitative analysis might be possible by 3D CL, which does provide dip data on planar features.

*4.4. Limitations and recommendations*

*4.4.1. Equipment limitations and suitable samples*

The combination of U-stage and EBSD measurements is powerful in the fact that it potentially can be applied to many samples. U-stage measurements can be performed on virtually all normal sized and normal thickness thin sections, with or without a cover plate. Although quite time-consuming (some PDF-bearing samples took several 10s of hours of measuring, because the orientation of some PDFs proved to be hard to constrain), it still remains the fastest way to measure many planes in a sample. The error is of course quite large, but there is no way to reduce this. Another disadvantage of the U-stage is that only about the middle 1/3 of a thin section can be covered. EBSD in the SEM can be applied on normal sized thin sections without a cover, when carefully polished and coated. Setting up and taking measurements, either manually or by automatic mapping, took about a day per considered sample. To cover all measured grains, a bit more time would have been necessary. As mentioned earlier, the error on EBSD is quite small, but there is a chance of misindexing Kickuchi patterns, giving erroneous crystal orientations.

Some samples are unsuitable for the combination of U-stage and EBSD. For example, samples with loose grains in an artificial matrix can maybe be covered with the U-stage (although hard), but are unsuitable for comparison with EBSD, as many grains will not be at the surface of such a thin section. This can be solved, and EBSD suitable samples can be made, but sometimes these are again not suitable for the U-stage. For these reasons, loose grain samples from the Geulhemmer Berg (Limburg, The Netherlands; possibly representing K/T boundary impact ejecta) were not included in this study.

A so called mixed sample is not problematic regarding the used devices, but in the analysis. (Old) shock-metamorphosed rocks may be overprinted by a later deformation event forming DL. When analysing such a sample, it most likely ends up somewhere in between pure impact and non-impact samples. In the U-stage analysis, this will probably not give a clear difference. The combination with EBSD data will also give a result somewhere in between (e.g. 50% indexing rate), for which it is very hard to decide whether an impact hypothesis is still viable. For such samples, the quantitative approach as descriped here is thus on its own not suitable, and qualitative and/or TEM-based studies might be necessary to unequivocally prove impact or non-impact origin. Mixed samples have not been encountered in this study.

*4.4.2. Data processing*

Processing the U-stage and EBSD data is quite time-consuming. After a method has been set up using one sample, the process however speeds up significantly for the others. One has to be very careful about rotations and corrections that have to be made. The symmetry of quartz is sometimes a blessing, as possible erroneous rotations (such as rotating 180° about the c-axis) do not really matter in the analysis of PDFs (see NSPT, figure 10). It can however be a burden while checking the actual correspondence of axes between the EBSD and the U-stage data. The current author has been very careful during the analysis, but it is advised for consecutive studies the methods are independently checked, i.e. by evaluating all steps from scratch.

*4.4.3. Recommendations for future research*

The results of this study display a great potential for combined EBSD and U-stage methods to distinguish quantitatively between shocked (impact) and non-shocked (endogenic, non-impact) metamorphosed quartz in thin sections. Beside impact confirmation, the results can also be used for shock barometry. For consecutive research, the following recommendations are given [this study between brackets], including some points made already:

- Investigate more impact and non-impact samples with both methods [Only 2 samples analysed with both methods].
- Investigate samples blindly, i.e. not knowing impact or non-impact origin on start. This includes investigating yet unknown or unconfirmed structures [Origin of all samples known in advance, and only confirmed impact and non-impact sites considered].
- Check the method of U-stage and EBSD data combination thoroughly.
- Check or bypass of analysis 2 for the EBSD data [Because the validity of the performed rotation is not certain yet].
- Use a good U-stage, to reduce errors in the U-stage data [Many problems were encountered during the use of the U-stage, and although probably all solved, a definitively correctly set-up U-stage gives more certainty].

## 5. Conclusion

Planar microstructures in quartz (PFs and PDFs), forming parallel to specific crystallographic planes, are considered as main evidence for meteorite impact. It sometimes proves to be hard to distinguish them qualitatively from endogenically formed DL with the optical microscope. Quantitative approaches using the U-stage are therefore often applied. The goal of this thesis was to check these classical U-stage techniques for quantitatively confirming impact planar features in quartz, and to see whether the addition of EBSD and CL data can provide more solid evidence. To this end, the following methods were considered, as summarized below, including the outcome. Six previously TEM confirmed impact samples, and three non-impact samples were used.

1) *The classical U-stage measurement technique, without indexing.*
   This technique only involves plotting angular data (between the quartz c-axis and poles to planar features), in binned intervals. No clear difference is observed between impact and non-impact samples. Previous literature reports distinct peaks only for impact samples, and a more bell-shaped form for non-impact samples. This can not be confirmed in this study. The only difference is a slight increase in higher angle (>30°) data for the non-impact samples, which is insufficient to be an actual criterion.

2) *The improved U-stage measurement technique, with indexing.*
   This technique involves so-called indexing of the U-stage data by a standard projection template (NSPT). Impact and non-impact samples index as similar planes, not providing a clear distinction. The non-impact samples have a slightly higher non-indexing rate, but again, this seems unsuitable as an actual criterion.

3) *The combination of U-stage and EBSD data.*
   EBSD data was obtained in the SEM, and provides information on the orientation of a quartz crystal, including its a-axes, hence the orientation of poles to crystallographic planes. No dip information on planes (e.g. PDFs) is available with the standard EBSD technique. Combination of the EBSD data with the U-stage data can however be used to confirm the parallelism of U-stage measured PDFs to the EBSD derived orientation of crystallographic planes. For an impact sample, PDFs could indeed be confirmed with non-indexing rates around 20%. For a non-impact sample, virtually no correspondence to PDF crystallographic planes was found, with non-indexing rates close to 90%.

4) *The addition of CL data, to see if it improves the result of method 3.*
   CL data was obtained in the SEM, and used to see if more planar features could be confirmed with this technique. Although sometimes features not observed in the U-stage were found, they could not be unequivocally assigned to certain crystallographic planes. The use of CL as in this study is therefore limited to recognising additional planes for another analysis in the U-stage. This is not advised, as taking CL data and going back to the U-stage is time-consuming and probably of little additional value.

In summary, contrary to previous reports, U-stage data alone is insufficient to prove impact definitively. The addition of EBSD data to the U-stage measurements is very promising for the analysed samples, as a clear distinction can be made between impact and non-impact samples. Some future improvement of the technique is recommended, e.g. by checking more samples and checking blindly, on samples with unknown origin.

**Acknowledgments**

I would like to thank Martyn Drury and Maartje Hamers for the set-up and supervision of this project, the availability of the samples, and their help and supervision with the various equipment. For their help with setting up a rather problematic U-stage and discussions on processing the data, I would like to thank Vincent Keizer, Hans de Bresser, Hans Avé Lallement and Ludovic Ferrière. Tim Wolterbeek's computational work on automating the rotation of the U-stage data was of great use, as it saved a lot of time, and proved to be more precise and accurate than a manual method. Further appreciation is extended to Gill Pennock for her "last minute" availability to help with an EBSD session on a non-impact sample, which improved the significance of the results in this thesis greatly. Finally, the authors of Stereo32, and especially Klaus Röller, are thanked for some discussions on data processing, and placing the full version of their great program at disposal to our research group free of charge. Of course, appreciation is also extended to many other people that helped in various stages of this thesis, but have not been mentioned separately above.

**Supplementary material**

Supplementary materials (original raw data, calculations, and formatted spreadsheets) are available digitally from the author (M.H. Voorn) and the supervisors (M.R. Drury and M.F. Hamers, Structural Geology and Tectonics research group, Earth Sciences department, Utrecht University, The Netherlands)

**References**

Akhavan, A.C., 2005-2010. The Quartz Page. http://www.quartzpage.de

Alexopoulos, J.S., Grieve, R.A.F. and Robertson, P.B., 1988. Microscopic lamellar deformation features in quartz: Discriminative characteristics of shock-generated varieties. Geology 16, 796-799

Alexopoulos, J.S., Grieve, R.A.F., and Robertson, R.B., 1989. Reply on comment on "Microscopic lamellar deformation features in quartz: discriminative characteristics of shock-generated varieties. Geology 17, 478-480

Alvarez, L.W., Alvarez, W., Asaro, F. and Michel, H.V., 1980. Extraterrestrial cause for the Cretaceous-Tertiary extinction. Science 208, 1095-1108

Avé Lallement, H.G., 2002. U(niversal)-Stage. Lecture notes to ESCI-568, Rice University, Houston, Texas, USA

Bohor, B.F., 1990. Shock-induced microdeformations in quartz and other mineralogical indications of an impact event at the Cretaceous-Tertiary boundary. Tectonophysics 171, 359-372

Bohor, B.F., Foord, E.E., Modreski, P.J. and Triplehorn, D.M., 1984. Mineralogic evidence for an impact event at the Cretaceous-Tertiary boundary. Science 224, 867-868

Bohor, B.F., Modreski, P.J. and Foord, E.E., 1987. Shocked quartz in the Cretaceous-Tertiary boundary clays: evidence for a global distribution. Science 236, 705-709

Bruijn, R.H.C., 2009. A comparison between deformation lamellae and planar deformation features in natural quartz using SEM and SEM with EBSD technology. MSc Thesis, internal report Department of Earth Sciences, University of Utrecht, The Netherlands

Carter, N.L. and Friedman, M., 1965. Dynamic analysis of deformed quartz and calcite from the Dry Creek ridge anticline, Montana. American Journal of Science 263, 747-785

Carter, N.L. and Officer, C.B., 1989. Comment on "Microscopic lamellar deformation features in quartz: discriminative characteristics of shock-generated varieties. Geology 17, 477-478

Carter, N.L., 1965. Basal quartz deformation lamellae - a criterion for recognition of impactites. American Journal of Science 263, 768-806

Carter, N.L., Officer, C.B., Chesner, C.A. and Rose, W.I., 1986. Dynamic deformation of volcanic ejecta from the Toba caldera: possible relevance to Creteceous/Tertiary boundary phenomena. Geology 14, 380-383

Castro, C.P. and Lagoeiro, L.E., 2009. U-stage and EBSD technique as complementary methods. Revista Brasileira de Geociências 39 (1), 112-128

Christie, J.M. and Raleigh, C.B., 1959. The origin of deformation lamellae in quartz. American Journal of Science 257, 385-407

Cordier, P., Vrána, S. and Doukhan, J.-C., 1994. Shock metamorphism in quartz at Sevetin and Susice (Bohemia)? A TEM investigation. Meteoritics 29, 98-99

Cortés, A.L., Díaz-Martínez, E., Sanz-Rubio, E., Martínez-Frías, J. and Fernández, C., 2002. Cosmic impact versus terrestrial origin of the Azuara structure (Spain): A review. Meteoritics and Planetary Science 37, 875-894

Dietz, R.S., 1947. Meteorite impact suggested by the orientation of shatter-cones at the Kentland, Indiana, disturbance. Science 105, 42-43

Earth Impact Database, 2010. Planetary and Space Science Centre, University of New Brunswick, Canada. http://www.unb.ca/passc/ImpactDatabase/

Ernstson, K. and Claudin, F., 2009. Ernston Claudin impact structures - The Azuara impact structure. http://www.impact-structures.com/spain/azuara.htm

Ernstson, K., Hammann, W., Fiebag, J. and Graup, G., 1985. Evidence of an impact origin for the Azuara structure (Spain). Earth and Planetary Science Letters 74, 361-370

Fairbairn, H.W., 1941. Deformation lamellae in quartz from the Ajibik formation, Michigan. Geological Society of America Bulletin 49, 1723-1746

Ferrière, L., 2008. Shock metamorphism and geochemistry of impactites from the Bosumtwi impact structure. PhD Thesis, Universität Wien.Fakultät für Geowissenschaften, Geographie und Astronomie http://othes.univie.ac.at/3342

Ferrière, L., Morrow, J.R., Amgaa, T. and Koeberl, C., 2009. Systematic study of universal-stage measurements of planar deformation features in shocked quartz: implications for statistical significance and representation of results. Meteoritics and Planetary Science 44 (6), 925-940

French, B.M. and Koeberl, C., 2010. The convincing identification of terrestrial meteorite impact structures: what works, what doesn't, and why. Earth-Science Reviews 98, 123-170

French, B.M., 1998. Traces of catastrophe - a handbook of shock-metamorphic effects in terrestrial meteorite impact structures. Lunar and planetary institute, Houston

Goltrant, O., Cordier, P. and Doukhan, J.-C., 1991. Planar deformation features in shocked quartz; a transmission eletron microscopy investigation. Earth and Planetary Science Letters 106, 103-115

Goltrant, O., Leroux, H., Doukhan, J.-C. and Cordier, P., 1992. Formation mechanisms of planar deformation features in naturally shocked quartz. Physics of the Earth and Planetary Interiors 74, 219-240

Götze, J., 2004 (March). Cathodoluminescence in geosciences. Lecture notes/Presentation slides of short course, Warsaw University. http://www.geo.uw.edu.pl/ERASMUS/files/Basics_of_luminescence.pdf

Grieve, R.A.F., Alexopoulos, J.S. and Robertson, R.B., 1989. Reply on comment on "Microscopic lamellar deformation features in quartz: discriminative characteristics of shock-generated varieties. Geology 17, 868-870

Grieve, R.A.F., Langenhorst, F. and Stöffler, D., 1996. Shock metamorphism of quartz in nature and experiment: II. Significance in geoscience. Meteoritics and Planetary Science 31, 6-35

Gucsik, A., 2009. Shock metamorphism of terrestrial impact structures and its application in the Earth and planetary sciences. In: Gucsik, A. (eds), Cathodoluminescence and its application in the planetary sciences. Springer-Verlag Berlin Heidelberg

Haff, J.C., 1940. Use of the Wulff net in mineral determination with the universal stage. American Mineralogist 24, 689-707

Hansen, E. and Borg, I.Y., 1962. The dynamic significance of deformation lamellae in quartz of a calcite-cemented sandstone. American Journal of Science 260, 321-336

Humphreys, F.J., 2001. Review: Graind and subgrain characterisation by electron backscatter diffraction. Journal of Materials Science 36, 3833-3854

Ingerson, E. and Tuttle, O.F., 1945. Relations of lamellae and crystallography of quartz and fabric directions in some deformed rocks. American Geophysical Union Transactions 26, 95-105

Kile, D.E., 2009. The universal stage: the past, present, and future of a mineralogical research instrument. Geochemical News 140, 1-21
http://www.geochemsoc.org/publications/geochemicalnews/gn140jul09/theuniversalstage.htm

Koeberl, C., 2002. Mineralogical and geochemical aspects of impact craters. Mineralogical Magazine 66 (5), 745-768

Langenhorst, F. and Deutsch, A., 1996. The Azuara and Rubielos structures, Spain: twin impact craters or Alpine thrust systems? TEM investigations on deformed quartz disprove shock origin. Lunar and Planetary Science 27, 725-726

Langenhorst, F., 1994. Shock experiments on pre-heated α- and β-quartz: II. X-ray and TEM investigations. Earth and Planetary Science Letters 128, 683-698

Langenhorst, F., 2002. Shock metamorphism of some minerals: basic introduction and microstructural observations. Bulletin of the Czech Geological Survey 77 (4), 265-282

Leroux, H., Reimold, W.U. and Doukhan, J.-C., 1994. A TEM investigation of shock metamorphism in quartz from the Vredefort Dome, South Africa. Tectonophysics 230, 223-239

McCall, G.J.H., 2009. Half a century of progress in research on terrestrial impact structures: a review. Earth-Science Reviews 92, 99-116

Parker, R.B. and Toots, H., 1989. Comment on "Microscopic lamellar deformation features in quartz: discriminative characteristics of shock-generated varieties. Geology 17, 868-870

Passchier, C.W. and Trouw, R.A.J., 1998. Microtectonics. 2nd corrected reprint. Springer-Verlag Berlin Heidelberg

Randle, V., 1992. Microtexture determination and its applications. The institute of materials 510, London

Reimold, W.U., 2007. The impact crater bandwagon (some problems with the terrestrial impact cratering record). Meteoritics & Planetary Science 42, 1467-1472

Röller, K. and Trepmann, C.A., 2008. Stereo32 v1.01 Software and helpfile. Ruhr-Universität Bochum, Institut für Geologie, Mineralogie & Geophysik. Software available for download at http://www.ruhr-uni-bochum.de/hardrock/downloads.htm

Schwarz, A.J., Kumar, M., Adams, B.L. and Field, D.P. (eds), 2009. Electron backscatter diffraction in materials science. 2nd Edition. Springer Science+Business Media, LLC, New York

Stadelmann, P.A., 2010. Weber Indices (HKIL to HKL). CIME website,
http://cimewww.epfl.ch/people/stadelmann/jemswebsite/Notes/WeberIndices.html

Stöffler, D. and Langenhorst, F., 1994. Shock metamorphism of quartz in nature and experiment: I. Basic observation and theory. Meteoritics 29, 155-181

Trepmann, C.A. and Spray, J.G., 2006. Shock-induced crystal-plastic deformation and post-shock annealing of quartz: microstructural evidence from crystalline target rocks of the Charlevoix impact structure, Canada. European Journal of Mineralogy 18, 161-173

Trepmann, C.A., 2008. Shock effects in quartz: compression versus shear deformation - an example from the Rochechouart impact structure, France. Earth and Planetary Science Letters 267, 322-332

Trepmann, C.A., 2009. Shock effects and pre-shock microstructures in hydrothermal quartz veins from the Rochechouart impact structure, France. Journal of Structural Geology 31, 1183-1196

Vernooij, M.G.C. and Langenhorst, F., 2005. Experimental reproduction of tectonic deformation lamellae in quartz and comparison to shock-induced planar deformation features. Meteoritics and Planetary Science 40 (9/10), 1353-1361

Von Engelhardt, W. and Bertsch, W., 1969. Shock induced planar deformation structures in quartz from the Ries crater, Germany. Contributions to Mineralogy and Petrology 20, 203-234

# Appendix:
# Use of the Universal Stage (U-stage) for uniaxial crystals

## Introduction

*The Universal Stage*

The Universal Stage, or U-stage in short, is a device that can be mounted on an optical microscope. The stage has several axes of rotation, in addition to the microscope table itself – the only axis of rotation for a normal optical microscope. The additional axes increase observational power on a thin section (TS) to the third dimension, and allow quantification of optical and geometric features in the thin section. This guide describes how the U-stage should be mounted and centred on the microscope, and how the stage can be used to measure the optic axis (related to the crystallography) of uniaxial crystals (e.g. quartz), and planar features (e.g. Böhm lamellae, Planar Deformation Features). For biaxial crystals, the reader is referred to other literature (e.g. Avé Lallement, 2002).

Several types of U-stages have been manufactured over the years (manufacturing ceased in the late 1990's). In this guide, the most common Leitz 4-axes U-stage is used, although most steps should be applicable to other U-stages as well. Figure U1 shows the stage indicating its rotational axes and corresponding lock knobs, and its measuring arcs.

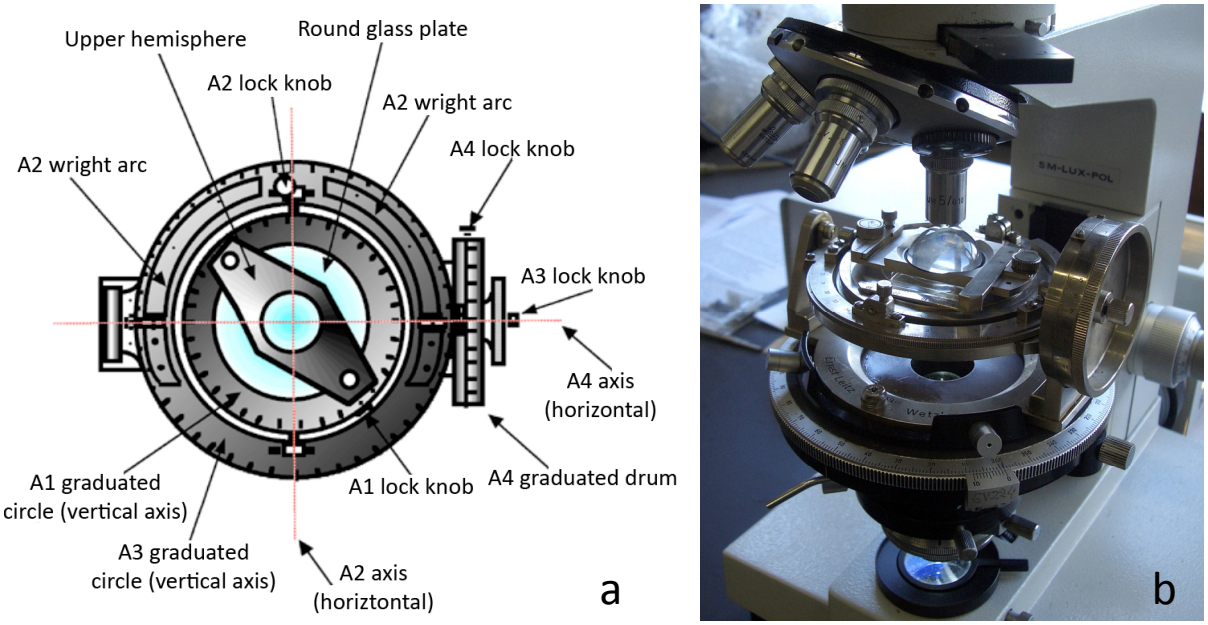


**Figure U1 a)** Top view diagram of the 4-axes universal stage, indicating the various axes, knobs and arcs needed for measurement. The A5 axis (microscope table) is not shown. After Kile (2009).
**b)** Mounted Leitz universal stage, including sample, on a Leitz optical microscope, at Utrecht University, Structural Geology and Tectonics Research Group.

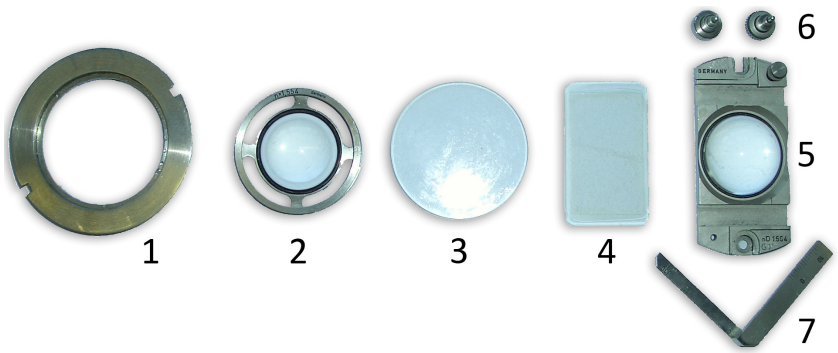


**Figure U2** Some of the equipment needed with the U-stage, in order of mounting:
1) Sample mounter
2) Lower hemisphere
3) Round glass plate
4) Thin section
5) Upper hemisphere
6) Sample mounter screws
7) Perpendicular hook

In different literature, different terminology is used for the axes, summarised in table U1. In this guide, I use the Berek notation, which counts the axes from inside outwards.

**Table U1** Notations for U-stage axes

| Description | Abbreviation | Berek | Reinhard | Fedoroff-Nikitin |
|---|---|---|---|---|
| Inner vertical or normal axis | IV | A1 | N | N |
| Inner horizontal or "North-South" | NS | A2 | H | H |
| Outer vertical or auxiliary axis | OV | A3 | A | M |
| Outer horizontal or "East-West" | EW | A4 | K | J |
| Microscope axis | MA | A5 | M | - |

Beside the rotational part of the U-stage, the following equipment is needed:

- Mounting screws (normal M4 screws fit as well) [Visible in figure U1b].
- Mounting or base plate with centring screws (optional/not available on all stages) [Visible in figure U1b].
- "Sample mounter", used to screw sample and spheres on, and to adjust sample height (by its threaded ring) [Figure U2-1].
- Round glass plate (fits in sample mounter) [Figure U2-2].
- Upper and lower hemisphere of a refractive index as close to the mineral of interest (n = 1.55 is usually widely available and mostly used for quartz), and corresponding screws [Figure U2-3 and U2-5].
- Oil of a refractive index as close to the mineral of interest (glycerine can be used for quartz), and a possibility to apply it in small droplets.
- Ethanol, acetone or similar to clean thin section and U-stage parts after use.
- Two small "screwdrivers" to centre objectives.
- Perpendicular hook (optional, fits in large upper hemispheres, very useful to ensure the long axis of the TS remains parallel to "North" of the microscope) [Figure U2-7]

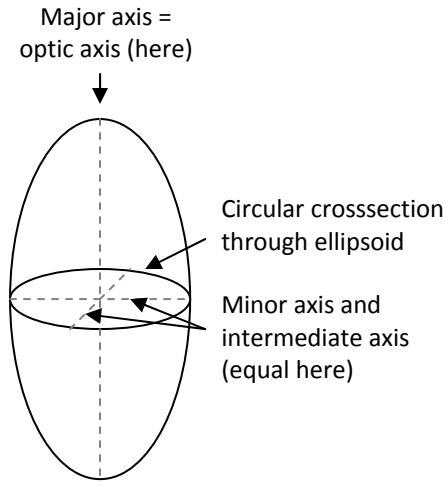


**Figure U3** Indicatrix for a uniaxial mineral. The major axis coincides with the optic axis (=perpendicular to a circular cross-section through the indicatrix). The minor and intermediate axes therefore also lie within this cross-section.

*Background on optic axes*

The indicatrix of a crystal is an ellipsoid representing the orientation and relative magnitude of its refractive indices (that indicate how the speed of light is changed when it travels through a material). The ellipsoid is described by three separate axes. When all axes are equal (hence the refractive index is the same in all directions), the material is isotropic. When two axes are equal, there is one single symmetry axis (perpendicular to the circular cross section through such an ellipsoid). This is called the optic axis, and the material is named uniaxial. See figure U3. This is for example the case with quartz, where the optic axis is parallel to the crystallographic c-axis. Materials for which the indicatrix has three distinct axes are called biaxial (referring to the two optical axes perpendicular to the circular cross sections through such an ellipsoid).

In an optical microscope, the light is polarised in one direction (EW) below the sample. When the cross-polariser is turned on, the light is polarised above the sample, perpendicular (=NS) to the first polarising direction. If the sample consists of an optically isotropic material (e.g. glass or an isotropic mineral), the polarisation direction of the light going through the sample is not changed. With the second polariser on, the material goes black in microscope view (the mineral goes extinct), in every orientation. For anisotropic (uni- or biaxial) minerals, due to their different refractive indices in different directions, the light is split into two different rays, that vibrate in planes perpendicular to each other (i.e. the light is polarised within the crystal). This process is called double refraction or birefringence. When exiting the mineral, the light seen is the combination of the two vibrational directions. Above steps are shown schematically in figure U4a. In plane polarised light (cross-polariser not turned on) there is no effect on the colours when rotating about the microscope axis, for many minerals (e.g. quartz). In other minerals, different colours can be absorbed along the different ray paths, resulting in different colours when rotating about the microscope axis; a process termed pleochroism. With the cross-polariser on, only light with a NS vibrational direction is let through. When indeed two combined perpendicular vibration directions exit the mineral, there is always a NS component to it, hence the mineral appears coloured in microscope view. The colour of the mineral in XPL when the most amount of light is let through is called the birefringence colour of the mineral. The birefringence colour thus is a representation of the difference in speed between the two split rays in the sample. It occurs in different orders, as visible on a birefringence colour chart.

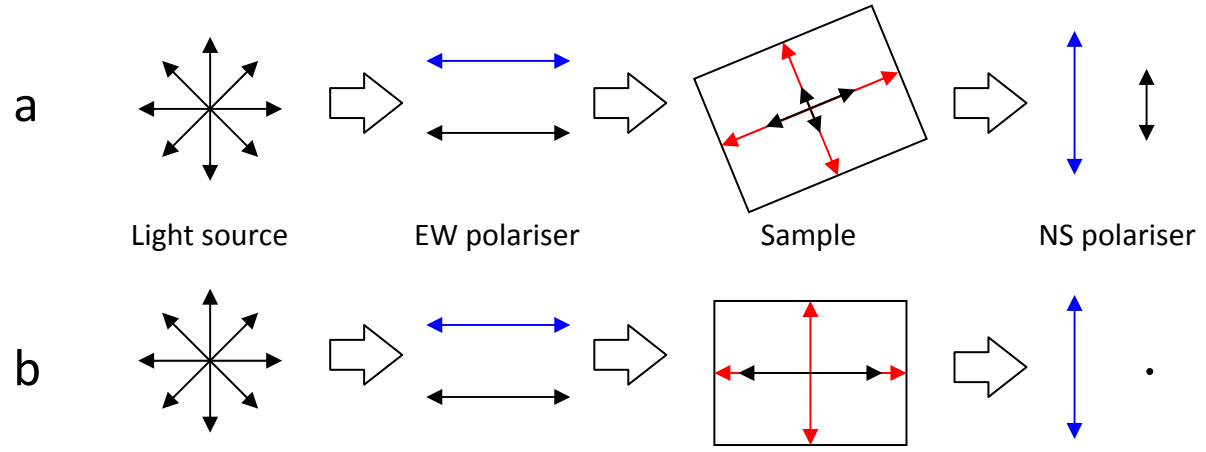


**Figure U4** Sketch of the polarising steps in an optical microscope, for anisotropic minerals. Black arrows represent (visible) light vibration directions. Blue arrows represent the vibration directions of the polarisers in the optical microscope. Red arrows represent vibration directions within the crystal.
**a)** General case **b)** One of the crystal vibration directions parallel to the first polariser (extinction)

The gypsum plate for optical microscopes is designed so the difference between the two rays is represented by precisely one birefringence colour. When inserted in the optical microscope, it either adds or subtracts one birefringence order to the birefringence colour of the grain of interest, dependent on the orientation of the sample. Quartz in a thin section of normal thickness (~30µm) has a 1$^{st}$ order grey birefringence colour. When the gypsum plate is inserted and addition occurs, this becomes 1$^{st}$ order blue. When subtraction occurs, this becomes 1$^{st}$ order yellow (note that "below" 1$^{st}$ order black the same orders are present, but "mirrored" relative to the normal birefringence colour chart!). This addition or subtraction is important in a later stage, when using the U-stage.

A “special” case occurs when one of the vibration directions within the crystal lies exactly *within the (vertical) plane* of the EW-polariser. In this case, the light is *not* split into two directions within the crystal, but keeps vibrating in the EW plane, parallel to the crystal’s vibration direction. Hence, the light coming out of the crystal vibrates in the EW plane, and the mineral goes extinct with the cross-polariser on! This is shown in figure U4b. It should be evident from the figure the mineral goes extinct four times in a full revolution about the microscope table axis A5 or the inner vertical axis A1 of a U-stage. For a uniaxial crystal, this means the optical axis (hence the c-axis for quartz) lies within the vertical plane of the EW polariser twice in a full revolution. In the figure, the c-axis can be imagined to be the “long” direction of the grain. With the U-stage, it is now possible to rotate the c-axis *within* the EW polariser vertical plane to a horizontal or vertical position. In this manner, the actual position of the c-axis relative to the sample can be expressed in terms of angles.

*Note: it is convention to rotate the c-axis to the vertical position, or the horizontal EW direction. On the U-stage, it would equally well be possible to rotate to the vertical position, or the horizontal NS direction, but this is generally not done. Also note since only the range from 270 to 90° on the A1 axis of the U-stage is going to be used, only one of the situations where the c-axis lies within the EW polariser vertical plane remains!*

**Mounting and centring the U-stage**

*Important note: the author of this guide has little experience with changing objective heads, condensers etcetera. It is therefore assumed the special condenser and objectives for u-stages are already in place. Suitable orthoscopic, long working-distance objectives (usually shorter and thinner than normal optical microscope objectives, also shown in figure U1b) can be added if needed, but for the more advanced microscope operations the reader is advised to consult someone with more expertise, if necessary.*

1) If the optional base plate is available, loosen its centring screws and place the U-stage on the base plate. Make sure the U-stage fits tightly and can not wobble, and the mounting holes of the base plate and the U-stage lie on top of each other.
2) Screw the U-stage onto the mounting holes of the microscope table using the mounting screws. Again, make sure the U-stage fits tightly and can not wobble.
3) Fit a sample in the U-stage (see later section!!).
4) Centre each installed objective using the two small screwdrivers corresponding to the objective head:
    a. Make sure the stage is horizontal (A2=0°, A4=0°), and perpendicular (A1=0°, A3=270°, A5=360 or 0°).
    b. Insert the screwdrivers in the slots for the objective that has to be centred.
    c. Centre the crosshair (by sliding the thin section!) on a point in the thin section that can easily be recognised, e.g. a triple junction of grains. This is position P.
    d. Rotate about A5 to check if crosshair stays at position P. If not, rotate by 180° on A5. The new position of the crosshair is Q.
    e. Move the crosshair (using the screwdrivers!) to a new position R, halfway on a straight line between P and Q.
    f. Rotate about A5 to check if crosshair stays at position R (or slide the thin section to another position first if R is not suitable to check this). If not, repeat steps c-f until it the crosshair stays centred .
5) Centre the U-stage. This is done in a similar manner as step 4, except now A5 stays fixed at 360 or 0°, rotation is done about A1 and the centring screws of the U-stage base plate are used instead of the screwdrivers! If no base plate with centring screws is installed, centring is done by sliding the U-stage manually over the microscope table, with the mounting screws a bit loosened. At the end of this step, the mounting screws can be screwed onto the microscope table tightly. Note: never do steps 4 and 5 in reverse order.
6) Make sure rotation about the A2 and A4 axes is parallel to the crosshair, and A2 and A4 are perpendicular:
    a. Keep all axes in their fixed positions (A1=0°, A2=0°, A3=270°, A4=0°, A5=360 or 0°). Bring the microscope table to a very low position and try to focus on dust particles on top of the upper hemisphere. If this is impossible without crashing into the microscope, try a small upper hemisphere.
    b. Rotate about A4: dust particles should move parallel to the crosshair from top to bottom of the field of view. If not: rotate about A5 until the particles move parallel along the crosshair when rotating on A4. Fix the A5 axis in this new position.
    c. Fix A4 at 0° and rotate about A2. Dust particles should move parallel to the crosshair from left to right in the field of view. If not, A2 and A4 are not orthogonal. This can be adjusted by rotating about A3. When OK, fix A3.
    d. Repeat/combine step b and c until A2 and A4 are perpendicular (dust particles move parallel the crosshairs in both directions). A3 stays fixed and is not used

again. On A5, mark the new "0-point" (see figure U5). For example, previously 0 corresponded to 360 or 0° on the arc of the microscope table; now 0 corresponds to 358°.

7) If necessary, the light source and the condenser can be centred (not described here).

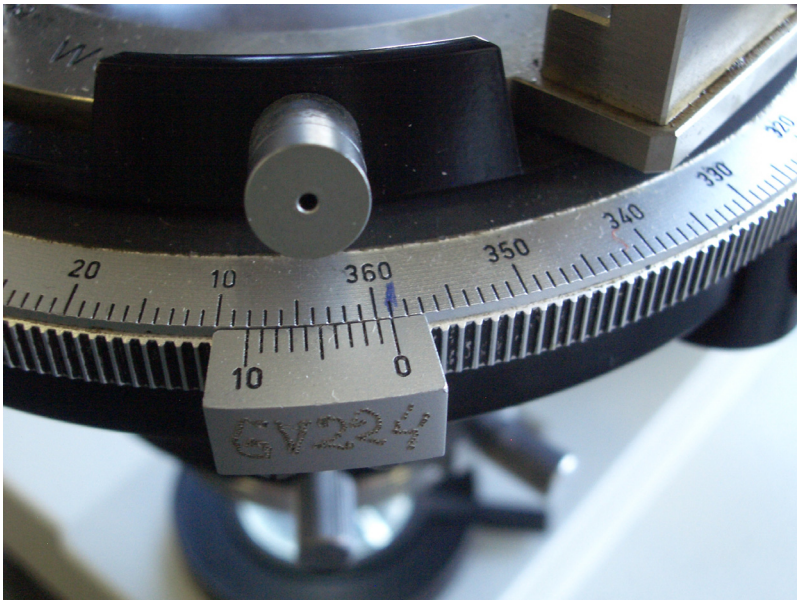


**Figure U5** New "0-point" indicated on the arc of the A5 axis. To ensure correct U-stage centring, it is crucial this point is indicated in this stage (if it differs from 360°), and used in all later stages.

**Fitting a sample in the U-stage**

1) Put the sample mounter in the U-stage in its lowermost position (NOTE: after screwing the sample mounter to its maximum, unscrew it a tiny bit to prevent jamming later).
2) Insert the lower hemisphere (check correct refractive index) in the sample mounter. Note this is a clamping system, and the lower hemisphere can fall through if pushed into position too hard!
3) Put 1-2 drops of oil/glycerine on top of the lower hemisphere, and put the round glass disc on top of it. Squeeze the lower hemisphere and the glass disc together gently and make sure the glass disc falls entirely within the sample mounter.
4) Put 1-2 drops of oil/glycerine on top of the glass disc, and lay the thin section on top of it. Note the sample side of the thin section must be pointing upwards when using large hemispheres! Also make sure you know how the sample is positioned, e.g. by always laying the thin section number at the bottom.
5) Put 1-2 drops of oil/glycerine on top of the sample, and put the upper hemisphere on top of it. The long ends of the thin section and the upper hemisphere are perpendicular. Screw the upper hemisphere onto the sample mounter with the provided screws (NOTE: it is best to screw both screws on at once, instead of one at a time). Screwing tighter and unscrewing controls the sample mobility when using the u-stage, but make sure the screws are not too tight to prevent the thin section from breaking!
6) The sample mounter controls the sample height. If the horizontal axes of rotation (A2 and A4) do not lie "within" the sample, the point of interest rotates out of microscope vision when rotating on A2 and A4. If the latter occurs, the sample should be unmounted, and the correct sample height can be achieved by unscrewing (or screwing tighter) the sample mounter. This is a process of trial and error; there seems to be no "trick" in literature to get the correct sample height immediately. For speed, one can try to get the correct sample height without using oil, or even by only laying the sample on top of the sample mounter, without spheres.

**Measuring the c-axis of uniaxial crystals**

The following steps should be followed to measure the c-axis position relative to the sample. Figure U6 shows the same steps in a schematic diagram.

1) Put the grain of interest under the crosshair by sliding the thin section between the glass hemispheres. Check if A5 is in its correct "0-point" position!
2) Turn on the cross-polariser, and insert the gypsum plate. When a birefringence order is added (the grain turns blue for normal ~30µm thick thin sections), rotate clockwise about A1 until the grains goes into extinction. If a birefringence order is subtracted (yellow for a ~30µm sample), rotate counterclockwise to extinction. Always stay between 270 and 90° (upper part) of the A1 axis! The above ensures the c-axis lies within the EW polariser vertical plane.
3) Rotate about A4 by at least 30°. The grain lights up again.
4) Keep A4 rotated, and rotate about A2 until the grain goes into extinction again.
5) Check if grain remains dark when rotating about A4, and adjust A2 rotation if necessary.
6) When OK, rotate A4 to 0° (horizontal) and lock the axis. Rotate about A5. If grain remains dark: vertical c-axis. If grain lights up: horizontal c-axis.
7) Read off and write down the azimuth (A1), the dip (A2, indicate whether the U-stage dips west (to the left) or east (to the right)), and whether the c-axis is horizontal or vertical (step 6); e.g. 78 / 20W / V.

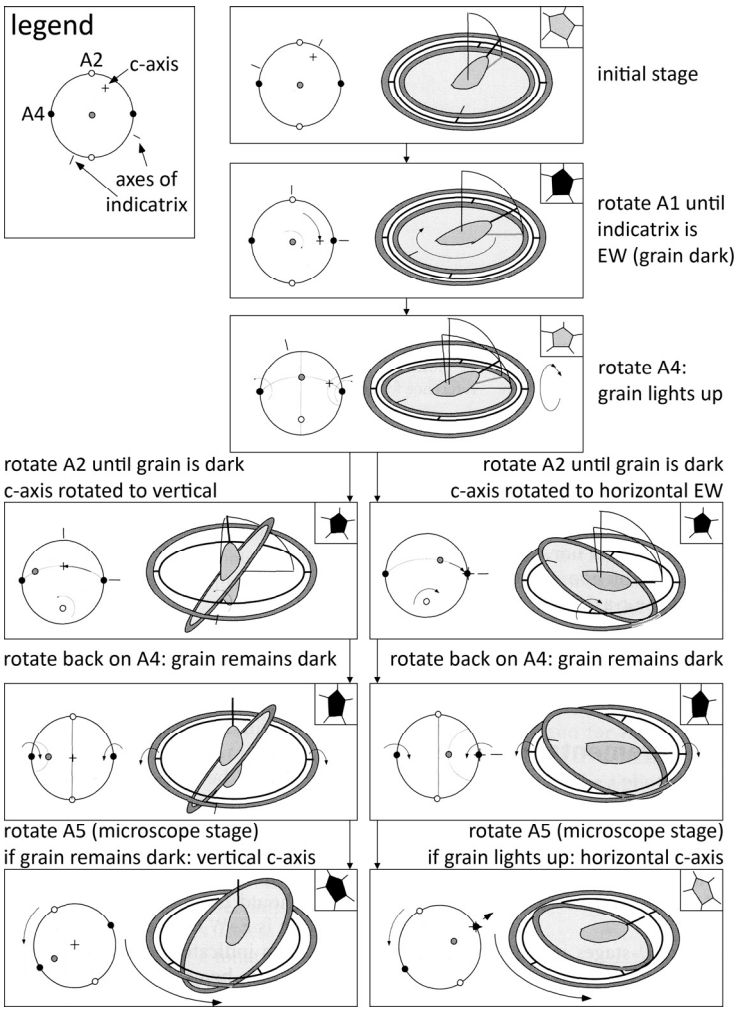


**Figure U6** Procedure for measuring c-axes of quartz with a U-stage. Different information is given in each window. Left: stereograms with the position and rotation angles of a c-axis and of U-stage axes, and the extinction positions of the indicatrix. Top right: the aspect of the grain to be measured as seen through the microscope. Centre: the U-stage and the indicatrix. Arcs represent the indicatrix indication in each case, the black bold line represents the c-axis, the bold grey line represents the projection of the c-axis in the horizontal plane. See text for further explanation. From: Passchier and Trouw (1998).

**Measuring planar features**

The orientation of planar features, e.g. deformation lamellae or Planar Deformation Features (PDFs; in impact metamorphosed rocks), that are visible on the thin section (2D section) as lines, can also be measured using the U-stage. When the instructions below are followed, measurements are performed in a similar manner as for the c-axis. They represent the position of the *pole* to the planar feature, relative to the sample. As we are usually interested in the relation between the planar feature and the c-axis, this way of measuring is the most convenient for processing the data in a later stage.

1) Put the grain of interest under the crosshair by sliding the thin section between the glass hemispheres. Check if A5 is in its correct "0-point" position, and keep A4 locked horizontally!
2) Rotate on A1 until the lines of interest lie parallel to the NS crosshair.
3) Rotate on A2 until the lines appear to be the thinnest possible. In that position, the observer looks parallel along the planar features. Note that when moving from a "too low" to a "too high" angle (or vice versa) on A2 the lines are usually at first not visible, than become visible but are a bit thick, than pass the "thinnest line" point, than become thick, and finally "vanish" again. Finding the thinnest line requires some practice or experience. It helps to start with a sample with clear thin planar features first. Furthermore, using a higher magnification works better in most cases, but sometimes only blurs the vision. Finally, it helps to keep changing focus a bit while trying to find the thinnest line. Some planar features even have a very narrow range of focus where they are visible, and sometimes this even differs from the focus for the entire grain!
4) Read off and write down the azimuth (A1) and the dip (A2, indicate whether the U-stage dips west (to the left) or east (to the right)). With this method we are looking along the planar feature (oriented NS), so the pole to the feature is always oriented EW horizontal. There is thus no need to write down "horizontal" or "vertical" as for the c-axis.

**Processing the data**

In most cases, the raw data from the U-stage has to be processed to be able to make further interpretations on the sample. First of all, the raw data can not directly be used in for example a stereogram, due to the way of measurement in a U-stage. Secondly, some calculations can be made on the relation between c-axes and planar features.

*From raw U-stage data to correctly oriented stereogram data*

For use in a stereogram, the raw U-stage data needs to be recalculated to normal stereogram data, e.g. like orientation data from a Silva compass. This recalculation should account for the following:

1) The view through the optical microscope effectively rotates the sample by 180°, relative to its orientation in normal view (not through a microscope).
2) The raw U-stage azimuth that is written down represents a NS orientation, while the poles we are interested in (e.g. c-axis, pole to a planar feature) lie EW.
3) As the sample is rotated while the A1 arc stays fixed, the raw U-stage azimuth data represents the azimuth of the long axis of the sample, relative to the feature (e.g. a lineation). We are however interest in the orientation of the feature, relative to the sample. This is graphically shown in figure U7.

4) The sample is rotated about axis A2. The dip written down is the dip of the sample, relative to the horizontally lying pole. Again, we are interested in the inverse: the orientation of the feature, relative to the sample. There also needs to be accounted for vertical poles (for c-axes only) separately.

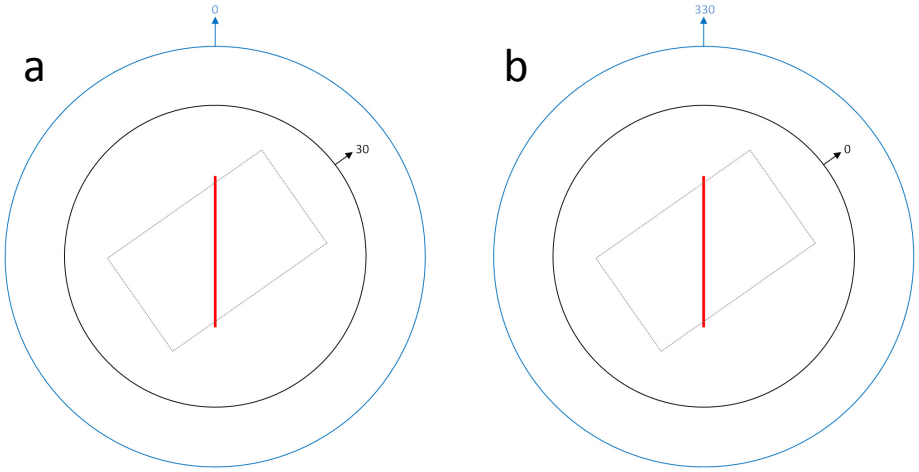


**Figure U7** Schematic diagram (not to scale) of Universal stage vs. the "normal" reference system.
**a)** U-stage system: Long axis of sample (30°) relative to lineation (0°)
**b)** Normal system: Long axis of lineation (330°) relative to sample (0°)

The solutions are as follows:

1) 180° rotation.
2) 90° rotation.
3) "Mirroring" the azimuth, using new azimuth = 360° - old azimuth (see figure U6).
4) For horizontal poles, "E" becomes "W" and vice versa. For vertical poles, "E" and "W" stay the same, but the dip changes by new dip = 90° - old dip.

Above solutions of course interfere with each other. The following recalculation scheme (table U2) accounts for this, with the reference direction parallel to the thin section, pointing away from the engraved sample number (see note below):

**Table U2** Recalculation scheme for raw U-stage data (vertical applies on c-axes only)

| Orientation of pole | U-stage dip direction | U-stage azimuth range | New azimuth | New dip |
|---|---|---|---|---|
| Horizontal | West | 0 ≤ azimuth ≤ 90 | 90 – azimuth | Dip (no change) |
| Horizontal | West | 90 < azimuth <360 | 450 – azimuth | Dip (no change) |
| Horizontal | East | 0 ≤ azimuth ≤ 270 | 270 – azimuth | Dip (no change) |
| Horizontal | East | 270 < azimuth < 360 | 630 – azimuth | Dip (no change) |
| Vertical | West | 0 ≤ azimuth ≤ 270 | 270 – azimuth | 90 – dip |
| Vertical | West | 270 < azimuth < 360 | 630 – azimuth | 90 – dip |
| Vertical | East | 0 ≤ azimuth ≤ 90 | 90 – azimuth | 90 – dip |
| Vertical | East | 90 < azimuth <360 | 450 - azimuth | 90 – dip |

*Note the author of this guide has applied the steps on a sample in normal (non-microscope) view. For my research purpose (on PDFs in quartz), some rotations did not matter for the final result. Please check the recalculation below if the correct orientation is crucial, as I am especially not fully sure whether step 1 should be applied. The recalculation corresponds to a correction to the reference direction of 270° in Stereo32, which is correct if Stereo32 requires the reference direction in microscope view. The recalculation scheme is preferred by the author over using Stereo32 directly, as the scheme accounts for vertical poles as well.*

*Rotations and angular relations*

For many purposes, the angle between the c-axis and the pole of a planar feature is required. Furthermore, it is useful to rotate the c-axis to a standard position. It is convention to rotate the c-axis to the centre of a stereogram. The steps below describe how to bring the c-axis to this position and how related poles (i.e. poles to planar features in the same grain) should be rotated, in a stereogram (after Haff, 1940). Also see figure U8:

1) Put the c-axis and all other poles of interest on a stereonet.
2) Rotate the tracing paper so the c-axis lies on the equator.
3) Put the new c-axis (c') at the projection centre (the centre of the stereonet), and count the angle between c' and the old c-axis (c) along the equator.
4) Keep the tracing paper in the same position and rotate all related poles by the same angle, in the same direction, along the small-circle on which they lie. Note that when crossing the outer circle of the stereogram, counting continues on the other hemisphere (e.g. when moving from a point on the southern hemisphere to 200/0, counting continues at 20/0).

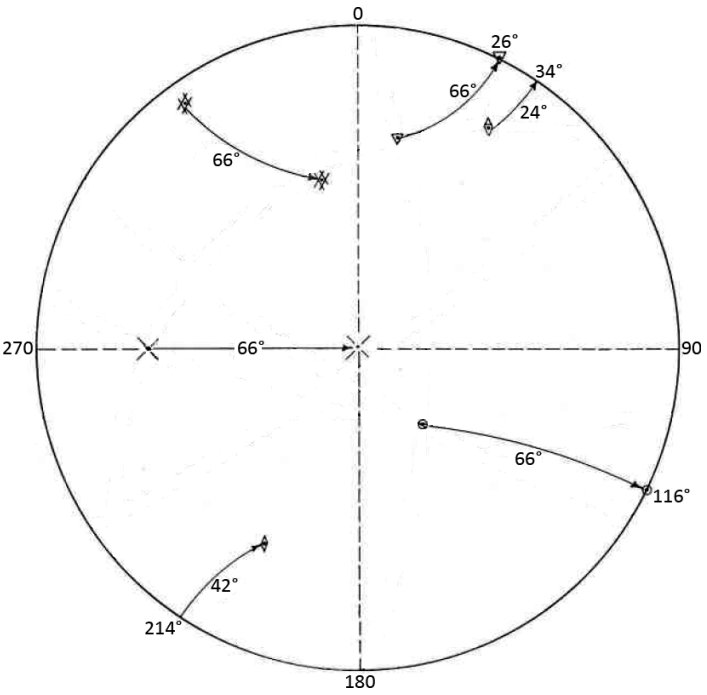


**Figure U8** Stereogram showing the method of shifting the reference plane pole to the projection centre, and related poles along with it, ensuring proper orientations. In the figure, the c-axis can be seen as the X, shifted 66° to the right. 4 related poles are therefore also shifted by 66° to the right, along their respective small circles. Especially note the shift of the "diamond-shaped" pole, as the transformation is done across the stereogram outer circle, hence moving from the northern hemisphere to the southern. Modified after Haff (1940)

The angle between the c-axis and a pole to a planar feature is now simply 90° minus the new dip of the planar feature. The method also allows for example to plot data from multiple grains in a single stereogram, as they are rotated to having the same c-axis now.

Above steps take quite a lot of time if they have to been done by hand. By recalculating the polar coordinates to 3D Cartesian vectors, a vector transformation can be applied. After recalculating these vectors back to polar coordinates, the same results are obtained as in the manual method. An Excel sheet for this purpose is available from the author. It is also possible to use stereographic software like Stereo32 to obtain the same results. It should be noted the computer and computational methods are more precise and accurate than the manual method. However, the manual method can always be used as a check, and is sometimes easier to understand.

**Unmounting a sample**

After every use, several parts of the U-stage need to be cleaned. This is also advised when an observer plans to continue working on a sample for example the next day. Keeping the sample in too long without moving it may result in jamming of the U-stage. To clean, take of the upper hemisphere, the sample, the round glass plate and the lower hemisphere, and lay them on a piece of paper. Wipe of any excess oil from the U-stage itself. Clean the parts taken off with e.g. ethanol or acetone, and dry using non-abrasive paper, to prevent scratches in the parts and of course the thin section itself.

**Known issues and shortfalls**

Several problems the author encountered before and during use of the U-stage are listed here.

*General*

- The U-stage can only be used to measure c-axes. The a-axes of quartz can not be measured using the device, so it is not possible to get a few 3D view of the crystallography of the sample.
- The U-stage has a limited range: it is usually not possible to reach every grain on a thin section, as you will not be able to rotate about A1 near the edge. Furthermore, the A2 and A4 axes can not always cover every possible orientation of the sample.
- The amount of used oil is very important. The authors experience is it is better to use a bit more oil than advised in many literature. Although the equipment gets a bit dirtier, it is less annoying and time-consuming than having to fully unmount the sample and re-apply oil when a sample jams due to a lack of oil. Also remove stickers from thin sections as these may cause U-stage jamming.
- For very thick samples, problems can occur with having not enough light and the sample height. Furthermore, the operator should be careful with the gypsum plate: the normal colour of quartz is now yellowish, and addition means for example a greenish colour, while subtraction results in white/greyish. It is easy to mix this up with "yellow" and "blue", so always keep the birefringence colour chart close to check addition and subtraction.
- Always make sure axes are locked quite tightly, so the U-stage can not rotate about one of its axes on its own, under gravity.

*My U-stage specific*

- It does not seem possible to get the sample height exactly right. It does work with the small hemispheres and the sample upside down, but then the hook to keep the sample orthogonal cannot be inserted. The sample mounter has even been thinned down to get better results, but it seems likely something else is wrong (maybe wrong objectives). Luckily, although taking measurements is sometimes a bit more tedious, the U-stage still seems to give the correct results.
- It was not possible to use the correct mounting screws for a U-stage as it would "wobble about" on the microscope table. Current set-up is the best achievement and works good, but requires the use of a screw-driver when the U-stage has to be centred, which introduces more problems. Furthermore, one should be careful the used screws are not too long, as this introduces problems when rotating about A5.
- Problems may occur with locking axes. The A5 axis already has to be locked very tight to have any effect, and the A2 axis seems to be at its maximum position already, while it still rotates.

**Short version of U-stage guide**

*Measuring the c-axis of uniaxial crystals*

1) Fix A5 (at correct 0-point) and position the grain by sliding.
2) Insert gypsum plate to see what happens to the birefringence colour. Addition: rotate clockwise about A1 to extinction. Subtraction: rotate counterclockwise. Stay between 270 and 90° on A1.
3) Rotate at least 30° about A4. The grain lights up.
4) Rotate about A2 until extinction. Check on A4 and fix A4 at 0°.
5) Rotate about A5. Grain lights up: horizontal c-axis. Extinction remains: vertical.
6) Write down azimuth (A1), dip (A2), dip direction (A2) and horizontal/vertical ("A5").

*Measuring poles to planar features*

1) Fix A5 (at correct 0-point) and A4, and position the grain by sliding.
2) Rotate about A1: lay lines NS parallel.
3) Rotate about A2: find thinnest line.
4) Write down azimuth (A1), dip (A2) and dip direction (A2).

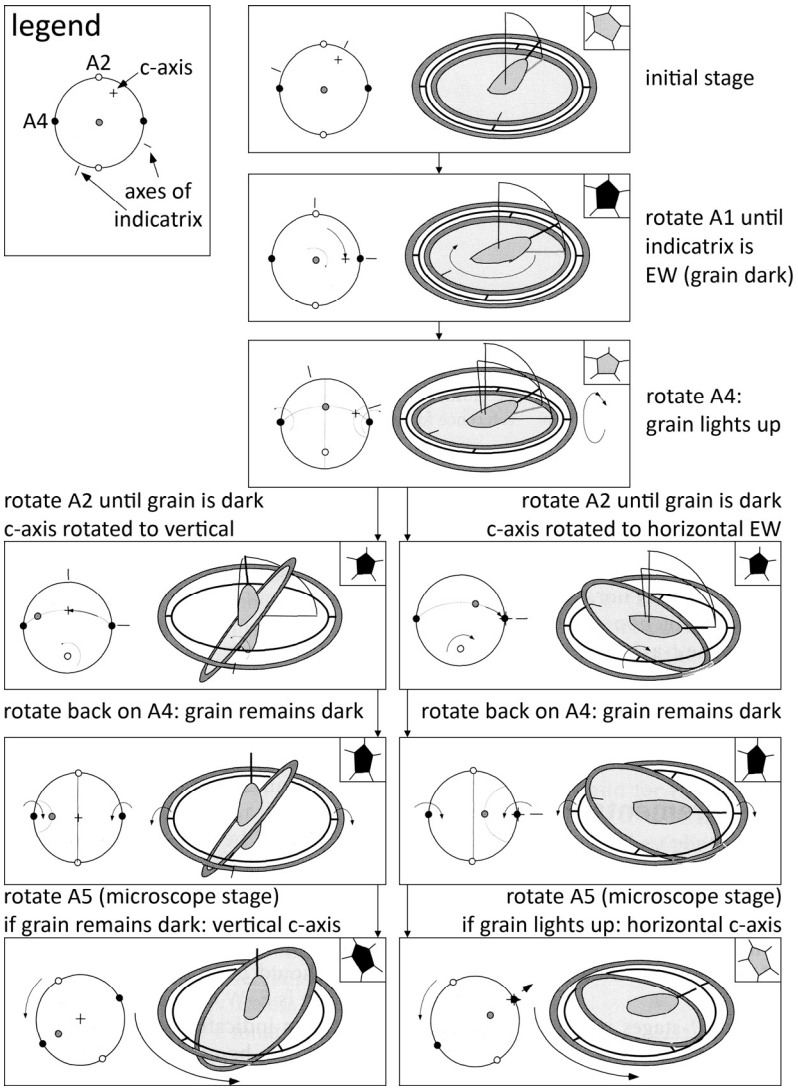


**Figure U6 (repeated)** Procedure for measuring c-axes of quartz with a U-stage. Different information is given in each window. Left: stereograms with the position and rotation angles of a c-axis and of U-stage axes, and the extinction positions of the indicatrix. Top right: the aspect of the grain to be measured as seen through the microscope. Centre: the U-stage and the indicatrix. Arcs represent the indicatrix indication in each case, the black bold line represents the c-axis, the bold grey line represents the projection of the c-axis in the horizontal plane. See text for further explanation. From: Passchier and Trouw (1998).

# U-stage planar feature measurements

Sample: Page: /

| Grain | C-axis | | | | Pole to planar feature | | | Comments |
|---|---|---|---|---|---|---|---|---|
| | *Strike* | *Dip* | *E/W* | *V/H* | *Strike* | *Dip* | *E/W* | |
| | | | | | | | | |
| | | | | | | | | |
| | | | | | | | | |
| | | | | | | | | |
| | | | | | | | | |
| | | | | | | | | |
| | | | | | | | | |
| | | | | | | | | |
| | | | | | | | | |
| | | | | | | | | |
| | | | | | | | | |
| | | | | | | | | |
| | | | | | | | | |
| | | | | | | | | |
| | | | | | | | | |
| | | | | | | | | |
| | | | | | | | | |
| | | | | | | | | |
| | | | | | | | | |
| | | | | | | | | |
| | | | | | | | | |
| | | | | | | | | |

Note: measurements as on universal stage, no correction! E/W = dip direction of universal stage. V/H = c-axis vertical or horizontal.

**Appendix: Meteoritical Society Poster**

The following page includes a poster presentation with the main results of this thesis, made by the author for the 73rd annual meeting of The Meteoritical Society in New York, July 26-30, 2010. It was presented/attended there by M.F. Hamers. If printed, please note the A0 size instead of A4 for the rest of this thesis.

# An improved way to confirm PDFs in quartz: U-stage and EBSD techniques combined

M.H. Voorn[1], M.F. Hamers[1*], M.R. Drury[1]

[1] Faculty of Geosciences, Department of Earth Sciences, Utrecht University, The Netherlands

* Corresponding author: hamers@geo.uu.nl

## Introduction

Unequivocal proof for Planar Deformation Features (PDFs) or Planar Fractures (PFs) in quartz is one of the most convincing lines of evidence for meteorite impact. Non-impact produced (tectonic) Deformation Lamellae (DL) - or Böhm lamellae - are sometimes misinterpreted as PDFs or PFs. Qualitative methods are usually insufficient to undeniably prove PDFs or PFs, and to distinguish them from DL, except for some Scanning and (expensive) Transmission Electron Microscopy (SEM and TEM) techniques. More quantitative approaches generally use the Universal Stage (U-stage) on the optical microscope, measuring the polar angle, between the quartz c-axis and poles to planar features. As PDFs and PFs only form parallel to certain crystallographic planes, polar angles should be restricted to the polar angles corresponding to these planes. DL, not forming parallel to crystallographic planes, should show a broader distribution of polar angles (see figure 1). In this study, 6 samples from previously TEM-confirmed impact sites and 3 non-impact samples were used to test the classical U-stage approach. On one impact and one non-impact sample, Electron Backscatter Diffraction (EBSD) on the SEM was performed. The EBSD data (providing c- and a-axes) and U-stage data (providing c-axis and poles to planar features) were combined, to see if better results could be obtained than with U-stage alone. U-stage and EBSD have been combined before (e.g. Trepmann & Spray, 2006), but to the authors' knowledge never on deformation lamellae samples.

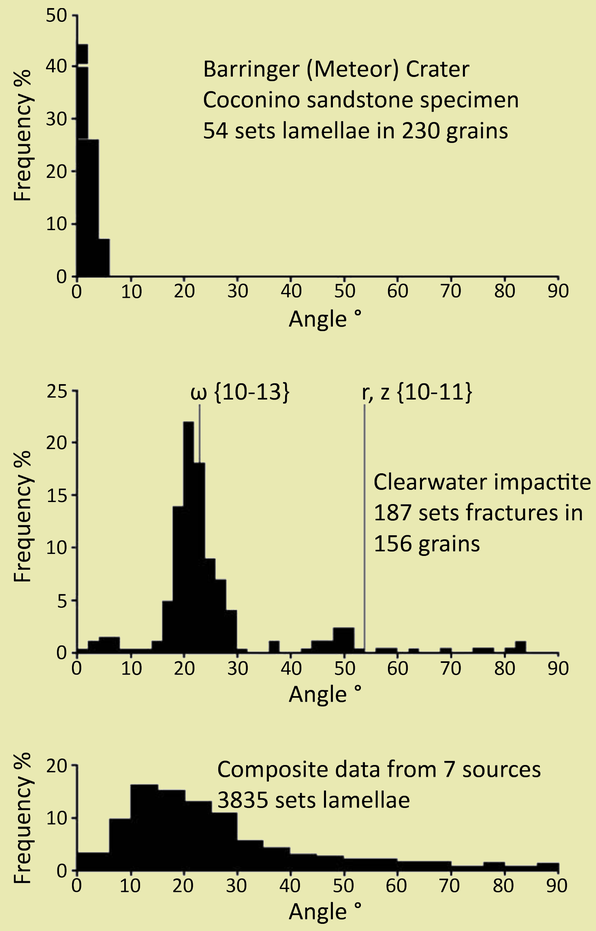


▲**Figure 1** Histograms of orientations of impact and non-impact planar microdeformation features in quartz grains, showing the frequency distribution of the polar angle (the angle between the quartz c-axis and the pole to the planar feature). a, b) The histograms for impact sites (PFs and PDFs in quartz) show clear peaks at distinct polar angles corresponding to certain crystallographic planes in the quartz crystal. 2° bins. c) The histogram for the non-impact samples (DL in quartz) shows a broad bell-shaped distribution without distinct spikes. Note this histogram is based on a lot more data from different sources, compared to a and b. 5° bins. From: French & Koeberl, 2010, after Carter, 1965.

## Methods

After U-stage and EBSD data acquisition, the following analyses were performed and graphs were produced:
1) U-stage data, with binned polar angles only 2) U-stage data, with planes indexed using the New Stereographic Projection Template (NSPT; Ferrière et al., 2009) 3) EBSD and U-stage combined, indexed with NSPT (method: see figure 2)

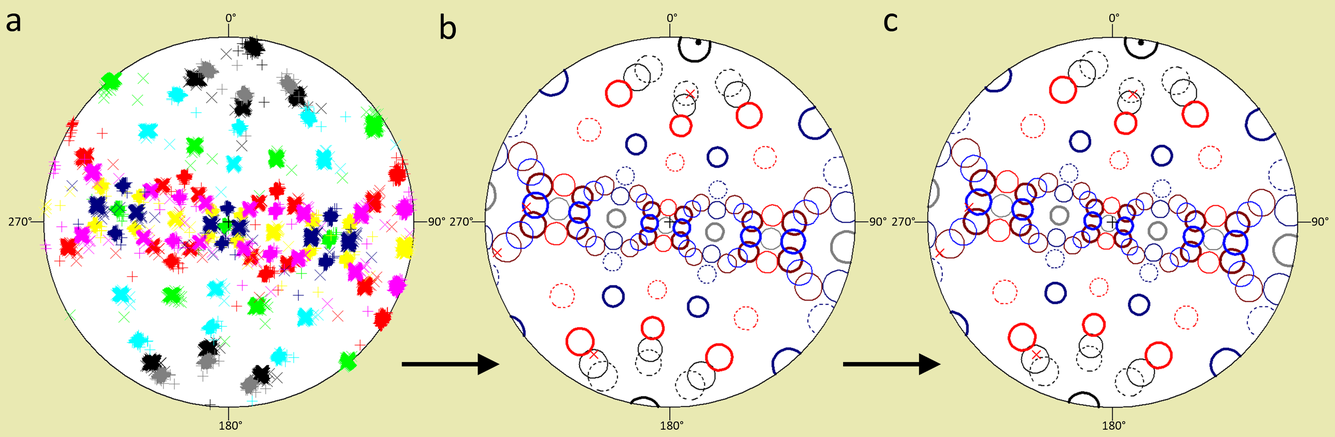


▲**Figure 2** Stereographic projections (lower hemisphere, equal angle) showing the method of combining EBSD and U-stage data for a grain in sample RI37 **a)** All poles to planes from EBSD data points plotted in same orientation as U-stage measurements. Not very suitable for further use, especially with more scatter on the data. **b)** NSPT fitted on figure 2a for indexing, combined with U-stage data. Black dot = U-stage c-axis, red crosses = U-stage poles to planar features. **c)** Same figure as 2b, but with NSPT slightly rotated to fit the U-stage c-axis. Optional step, validity needs to be checked. Stereographic projections created with Stereo32 software (© K. Röller & C.A. Trepmann, 2008)

## Results and discussion

Figure 3 shows some examples of the binned and indexed U-stage. The plots for impact and non-impact samples are very similar, both in the binned as the indexed form. This is not in line with previous reports (compare figure 1). Sample H4 (Vredefort) proves impact samples do not always have more sets/grain than non-impact samples. The only notable difference in the graphs is the unindexed rate: this is slightly higher for non-impact samples, but seems insufficient to be a criterion. Data from the U-stage only therefore do not seem to provide unequivocal evidence for PDFs.

Figure 4 shows an example for combined U-stage and EBSD data, for both an impact and a non-impact sample. The unindexed rate increases for both samples, but is extremely high for the non-impact sample. The addition of EBSD thus provides much stronger evidence for the presence of impact produced planar features than U-stage data alone.

Note this study focuses on quantitative results. In a qualitative way, it is virtually impossible to confuse the planar structures in the here investigated non-impact samples with PDFs or PFs. Furthermore, the origin of every sample was known in advance. It can however still be implied that quantitative results from the U-stage only are insufficient to (dis)prove impact.

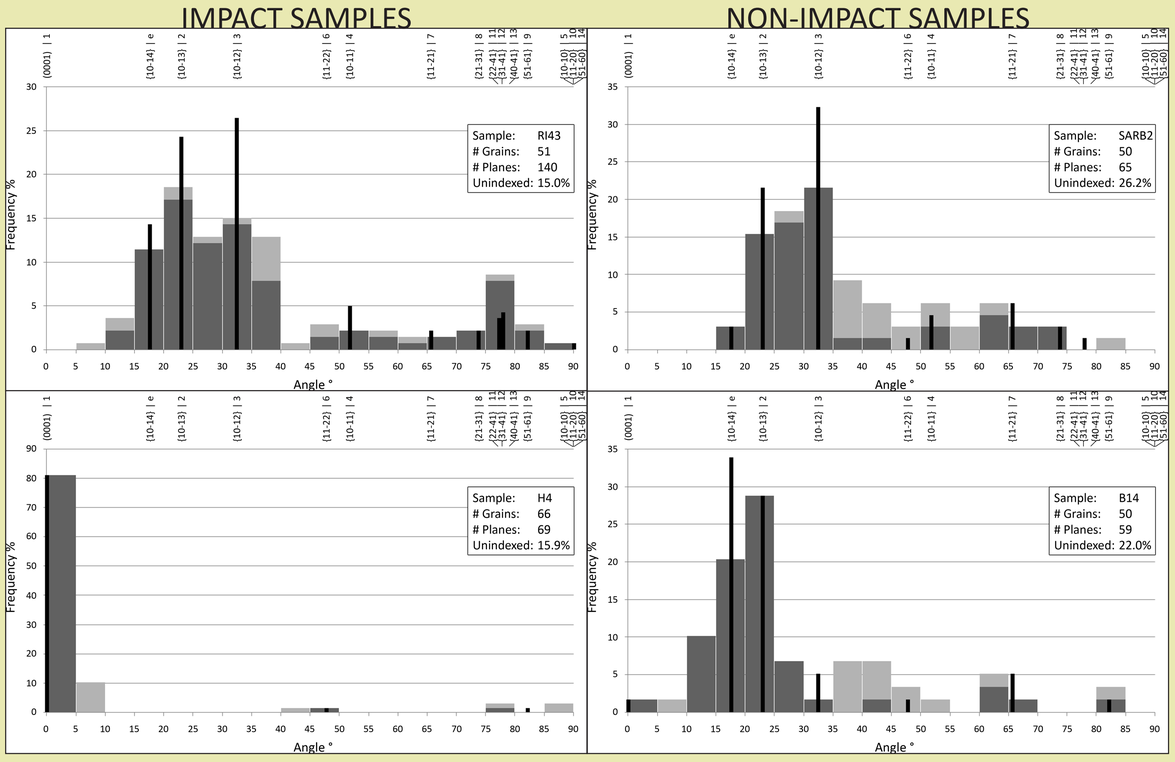


▲**Figure 3** Frequency distribution plots of planar microstructures in quartz grains, in some of the studied samples. Left: impact produced planar features (mainly PDFs, some PFs). Right: non-impact produced planar microstructures (mainly DL, some inclusion trails). The binned angular data shows the frequency distribution of the polar angle (the angle between the quartz c-axis and the pole to the planar feature). Dark grey bins: indexed angles; Light grey bins: unindexed angles. The black "spikes" show the frequency of indexed planes (indicated above) using the NSPT. Frequency is the so-called "absolute frequency" F of Ferrière et al., 2009. Generally differences between the studied impact and non-impact samples are minute. See text for further discussion.

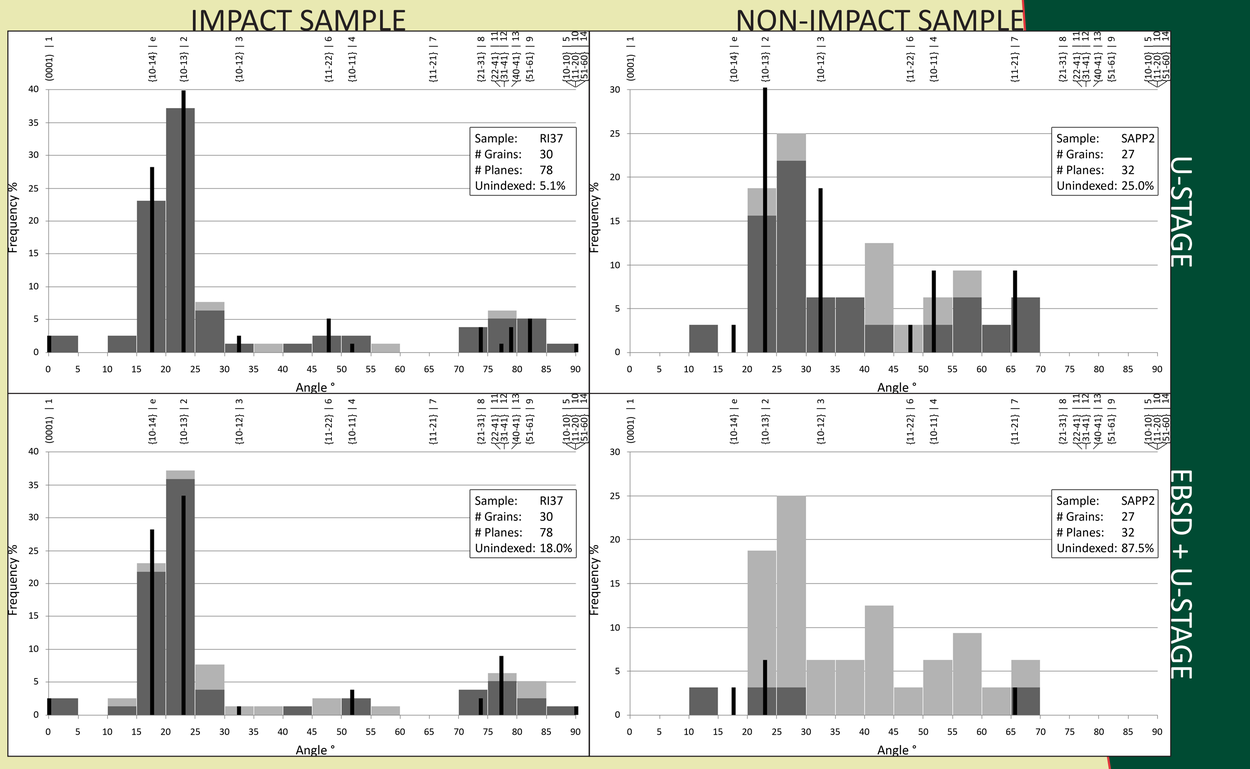


▲**Figure 4** Frequency distribution plots of planar microstructures in quartz grains, in some of the studied samples. Left: impact produced planar features (mainly PDFs, some PFs), in sample RI37. Right: non-impact produced planar microstructures (mainly DL, some inclusion trails), in sample SAPP2. Top: U-stage analysis only (only for grains later covered with EBSD). Bottom: EBSD and U-stage analysis, for grains covered with EBSD. Further legend like figure 3. Note the large difference in the unindexed rate between the lower two panels. See text for further discussion.

## Conclusions

- U-stage data alone is insufficient to (dis)prove shocked quartz
- Combined SEM-EBSD and U-stage data proves very promising in unequivocally distinguishing PDFs from tectonic deformation lamellae
- Combined EBSD/U-stage is potentially an alternative to TEM studies

Nederlandse Organisatie voor Wetenschappelijk Onderzoek

References:

- French, B.M. & Koeberl, C., 2010. Earth-Science Reviews 98, 123-170
- Carter, N.L., 1965. American Journal of Science 263, 768-806
- Trepmann, C.A. & Spray, J.G., 2006. European Journal of Mineralogy 18, 161-173
- Ferrière, L., Morrow, J.R., Amgaa, T. & Koeberl, C., 2009. Meteoritics and Planetary Science 44 (6), 925-940
- Röller, K. & Trepmann, C.A., 2008. Stereo32 v1.01 Software. Software available at http://www.ruhr-uni-bochum.de/hardrock/downloads.htm